

# *Lanthanide speciation in potential SANEX and GANEX actinide/ 2 lanthanide separations using Tetra-N-Donor extractants*

Article

Accepted Version

Whittaker, D. M., Griffiths, T. L., Helliwell, M., Swinburne, A. N., Natrajan, L. S., Lewis, F., Harwood, L. ORCID: <https://orcid.org/0000-0002-8442-7380>, Parry, S. A. and Sharrad, C. A. (2013) Lanthanide speciation in potential SANEX and GANEX actinide/ 2 lanthanide separations using Tetra-N-Donor extractants. *Inorganic Chemistry*, 52 (7). pp. 3429-3444. ISSN 0020-1669 doi: <https://doi.org/10.1021/ic301599y> Available at <https://centaur.reading.ac.uk/31184/>

It is advisable to refer to the publisher's version if you intend to cite from the work. See [Guidance on citing](#).

To link to this article DOI: <http://dx.doi.org/10.1021/ic301599y>

Publisher: American Chemical Society

All outputs in CentAUR are protected by Intellectual Property Rights law, including copyright law. Copyright and IPR is retained by the creators or other copyright holders. Terms and conditions for use of this material are defined in

the [End User Agreement](#).

[www.reading.ac.uk/centaur](http://www.reading.ac.uk/centaur)

## **CentAUR**

Central Archive at the University of Reading

Reading's research outputs online

# 1 Lanthanide Speciation in Potential SANEX and GANEX Actinide/ 2 Lanthanide Separations Using Tetra-N-Donor Extractants

3 Daniel M. Whittaker,<sup>\*,†</sup> Tamara L. Griffiths,<sup>†</sup> Madeleine Helliwell,<sup>‡</sup> Adam N. Swinburne,<sup>†</sup>  
4 Louise S. Natrajan,<sup>†</sup> Frank W. Lewis,<sup>§</sup> Laurence M. Harwood,<sup>§</sup> Stephen A. Parry,<sup>||</sup>  
5 and Clint A. Sharrad<sup>\*,†,#,⊥</sup>

6 <sup>†</sup>Centre for Radiochemistry Research, School of Chemistry, The University of Manchester, Oxford Road, Manchester M13 9PL, U.K.

7 <sup>‡</sup>School of Chemistry, The University of Manchester, Oxford Road, Manchester M13 9PL, U.K.

8 <sup>§</sup>Department of Chemistry, University of Reading, Whiteknights, Reading RG6 6AD, U.K.

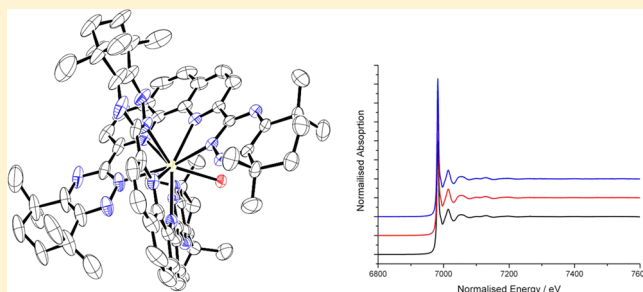
9 <sup>||</sup>Harwell Science and Innovation Campus, Diamond Light Source Ltd., Diamond House, Didcot, Oxfordshire OX11 0DE, U.K.

10 <sup>#</sup>School of Chemical Engineering and Analytical Science, The University of Manchester, Oxford Road, Manchester M13 9PL, U.K.

11 <sup>⊥</sup>Research Centre for Radwaste and Decommissioning, Dalton Nuclear Institute, The University of Manchester, Oxford Road,  
12 Manchester M13 9PL, U.K.

## 13 **S** Supporting Information

14 **ABSTRACT:** Lanthanide(III) complexes with N-donor ex-  
15 tractants, which exhibit the potential for the separation of  
16 minor actinides from lanthanides in the management of spent  
17 nuclear fuel, have been directly synthesized and characterized  
18 in both solution and solid states. Crystal structures of the Pr<sup>3+</sup>,  
19 Eu<sup>3+</sup>, Tb<sup>3+</sup>, and Yb<sup>3+</sup> complexes of 6,6'-bis(5,5,8,8-tetramethyl-  
20 5,6,7,8-tetrahydro-1,2,4-benzotriazin-3-yl)-1,10-phenanthroline  
21 (CyMe<sub>4</sub>-BTPhen) and the Pr<sup>3+</sup>, Eu<sup>3+</sup>, and Tb<sup>3+</sup> complexes of  
22 2,9-bis(5,5,8,8-tetramethyl-5,6,7,8-tetrahydro-1,2,4-benzotriazin-  
23 3-yl)-2,2'-bipyridine (CyMe<sub>4</sub>-BTBP) were obtained. The  
24 majority of these structures displayed coordination of two of  
25 the tetra-N-donor ligands to each Ln<sup>3+</sup> ion, even when in some cases the complexations were performed with equimolar amounts  
26 of lanthanide and N-donor ligand. The structures showed that generally the lighter lanthanides had their coordination spheres  
27 completed by a bidentate nitrate ion, giving a 2+ charged complex cation, whereas the structures of the heavier lanthanides  
28 displayed tricationic complex species with a single water molecule completing their coordination environments. Electronic  
29 absorption spectroscopic titrations showed formation of the 1:2 Ln<sup>3+</sup>/L<sub>N-donor</sub> species (Ln = Pr<sup>3+</sup>, Eu<sup>3+</sup>, Tb<sup>3+</sup>) in methanol when  
30 the N-donor ligand was in excess. When the Ln<sup>3+</sup> ion was in excess, evidence for formation of a 1:1 Ln<sup>3+</sup>/L<sub>N-donor</sub> complex  
31 species was observed. Luminescent lifetime studies of mixtures of Eu<sup>3+</sup> with excess CyMe<sub>4</sub>-BTBP and CyMe<sub>4</sub>-BTPhen in  
32 methanol indicated that the nitrate-coordinated species is dominant in solution. X-ray absorption spectra of Eu<sup>3+</sup> and Tb<sup>3+</sup>  
33 species, formed by extraction from an acidic aqueous phase into an organic solution consisting of excess N-donor extractant in  
34 pure cyclohexanone or 30% tri-*n*-butyl phosphate (TBP) in cyclohexanone, were obtained. The presence of TBP in the organic  
35 phase did not alter lanthanide speciation. Extended X-ray absorption fine structure data from these spectra were fitted using  
36 chemical models established by crystallography and solution spectroscopy and showed the dominant lanthanide species in the  
37 bulk organic phase was a 1:2 Ln<sup>3+</sup>/L<sub>N-donor</sub> species.



## 38 **I** INTRODUCTION

39 The reprocessing of irradiated spent nuclear fuel (SNF) has  
40 been performed since the 1940s, with the initial motivation to  
41 isolate plutonium for military purposes but more recently with  
42 the purpose to separate and recover both uranium and  
43 plutonium in order to maximize the resources available to  
44 generate civil nuclear energy.<sup>1,2</sup> Reprocessing can also reduce  
45 the volume of nuclear waste generated with high levels of  
46 radioactivity due to the presence of long-lived radionuclides.<sup>1,2</sup>  
47 This separation is most commonly performed by PUREX  
48 (Plutonium URanium EXtraction, also known as Plutonium

Uranium Reduction EXtraction), which is a biphasic solvent  
49 extraction process whereby {UO<sub>2</sub>}<sup>2+</sup> and Pu<sup>4+</sup>, from SNF  
50 dissolved in nitric acid (3–4 M), are extracted into an organic  
51 phase containing tri-*n*-butyl phosphate (TBP; Figure 1) in a  
52 hydrocarbon diluent (e.g., *n*-dodecane or odorless kero-  
53 sene).<sup>1–4</sup> The uranium and plutonium are transferred into  
54

**Special Issue:** Inorganic Chemistry Related to Nuclear Energy

**Received:** July 23, 2012

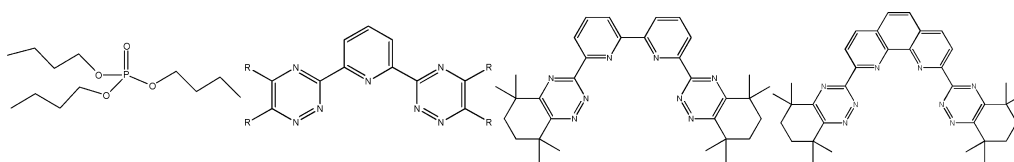


**Figure 1.** Structures of TBP (far left), BTP (center left), CyMe<sub>4</sub>-BTBP (center right), and CyMe<sub>4</sub>-BTPhen (far right).

55 the organic phase by forming charge-neutral complexes with  
 56 TBP (i.e.,  $[\text{UO}_2(\text{TBP})_2(\text{NO}_3)_2]$  and  $[\text{Pu}(\text{TBP})_2(\text{NO}_3)_4]$ ).<sup>1,3–5</sup>  
 57 The plutonium, after reduction to  $\text{Pu}^{3+}$ , and uranium are then  
 58 back-extracted into an aqueous phase for reuse. The aqueous  
 59 phase remaining after the initial separation, known as highly  
 60 active raffinate (HAR), contains over 99.9% of the fission  
 61 products (e.g., lanthanide isotopes, <sup>137</sup>Cs, <sup>90</sup>Sr, <sup>99</sup>Tc) and the  
 62 minor actinide activation products (neptunium, americium, and  
 63 curium) with decontamination factors of  $10^6$ – $10^8$  achieved by a  
 64 multistage separation process.<sup>1</sup> The long-term management of  
 65 HAR, after conversion into an appropriate wasteform, can be  
 66 extremely problematic, in part due to the presence of  
 67 americium and curium, which are highly radioactive and have  
 68 very long half-lives (up to  $10^5$  years).<sup>1,2</sup>

69 Considerable efforts have been made recently to develop  
 70 advanced separation methodologies in order to maximize fuel  
 71 resources and reduce the impact of nuclear waste while  
 72 providing a proliferation-resistant fuel cycle (i.e., no pure  
 73 plutonium is isolated).<sup>1,2,4,6–11</sup> This forms part of the  
 74 “Partitioning and Transmutation” strategy, where it is proposed  
 75 that all of the actinides in SNF, including the minor actinides,  
 76 can be separated and recycled as nuclear fuel. Another option is  
 77 to “burn” the separated actinides, which will also result in  
 78 conversion to short-lived fission product nuclides but without  
 79 nuclear energy production for public consumption. This  
 80 provides the added benefit of converting most of the long-  
 81 lived actinides in SNF to shorter-lived fission product nuclides  
 82 compared to current spent fuel management options. As a  
 83 result, the “Partitioning and Transmutation” strategy can  
 84 significantly reduce the time it takes for SNF to decay to  
 85 radioactivity levels of natural uranium and therefore the  
 86 necessary design lifetime of any nuclear waste repository.<sup>7–11</sup>

87 One of the major separation challenges that need to be  
 88 overcome for this strategy to be successful is the separation of  
 89 americium and curium from the lanthanide fission products.  
 90 This is because the high neutron absorption cross sections of  
 91 some of the lanthanide ions present in SNF both decrease the  
 92 flux in a reactor and create more activation products, thereby  
 93 making transmutation a less attractive option if the lanthanides  
 94 cannot be separated from the actinides.<sup>10</sup> Achieving this  
 95 separation is extremely difficult because of the chemical  
 96 similarities between americium, curium, and the lanthanides,  
 97 which all most commonly exist in the III+ oxidation state in  
 98 solution.<sup>12</sup> Consequently, organic molecules that can selectively  
 99 extract actinides, in particular  $\text{Am}^{3+}$  and  $\text{Cm}^{3+}$ , over the  $\text{Ln}^{3+}$   
 100 ions are of great interest, as is evident by the number of  
 101 different ligand systems and processes that have been  
 102 developed by various groups in the field of partition-  
 103 ing.<sup>2,4,6–10,12–22</sup> Examples include the TALSPEAK (Trivalent  
 104 Actinide Lanthanide Separation by Phosphorus reagent  
 105 Extraction from Aqueous Komplexes) process, which uses  
 106 diethylenetriaminepentaacetic acid in a lactic acid solution to  
 107 hold back  $\text{Am}^{3+}$  and  $\text{Cm}^{3+}$  in the aqueous phase while the  
 108 lanthanide ions are extracted into the organic phase containing  
 109 di(2-ethylhexyl)phosphoric acid,<sup>13,14</sup> and the TRUEX (TRANS-

Uranic EXtraction) process, where the addition of octyl-  
 (phenyl)-*N,N*-diisobutylcarboylmethylphosphineoxide to the  
 organic phase in the core PUREX process allows  $\text{Am}^{3+}$  and  
 $\text{Cm}^{3+}$  to be extracted alongside  $\{\text{UO}_2\}^{2+}$  and  $\text{Pu}^{4+}$ , leaving the  
 lanthanide ions and other fission products in the aqueous  
 phase.<sup>14,15</sup>

The SANEX (Selective ActiNide EXtraction) solvent  
 extraction process<sup>8,9</sup> aims to separate the minor actinides  
 americium and curium from the lanthanide fission products  
 remaining after plutonium and uranium removal by PUREX  
 and fission product separation (except the lanthanides) by  
 DIAMEX (DIAMide EXtraction)<sup>16</sup> using only carbon-, hydro-  
 gen-, oxygen-, and nitrogen-containing compounds as extrac-  
 tants, diluents, or phase modifiers. A class of molecules that  
 showed early promise for the selective extraction of  $\text{An}^{3+}$  over  
 $\text{Ln}^{3+}$  in a SANEX process were the tridentate 2,6-bis(5,6-  
 dialkyl-1,2,4-triazin-3-yl)pyridines (BTPs; Figure 1).<sup>7,17</sup> How-  
 ever, many of these extractant molecules suffered problems that  
 precluded them from use in plant-scale extractions including  
 poor stability, slow extraction kinetics, and inefficient back-  
 extraction due to high  $\text{An}^{\text{III}}$  affinities.<sup>7</sup> Further developments in  
 the use of triazinyl-based N-donor extractants for actinide/  
 lanthanide separations have led to the tetradentate ligand 2,9-  
 bis(5,5,8,8-tetramethyl-5,6,7,8-tetrahydro-1,2,4-benzotriazin-3-  
 yl)-2,2'-bipyridine (CyMe<sub>4</sub>-BTBP; Figure 1), which exhibits  
 significant potential for use in SANEX separations, with  
 separation factors for  $\text{Am}^{3+}$  over  $\text{Eu}^{3+}$  found to be  
 $\sim 150$ .<sup>7,18,19</sup> The CyMe<sub>4</sub>-BTBP extractant has been successfully  
 tested for the extraction of genuine actinide/lanthanide feed  
 through a 16-stage centrifugal contactor setup with excellent  
 recoveries for americium and curium (>99.9%) but has been  
 shown to undergo radiolytic degradation at doses that will be  
 encountered at the high minor actinide loadings obtained in the  
 reprocessing of, for example, fast reactor fuels.<sup>19</sup> The kinetics  
 for actinide extraction with CyMe<sub>4</sub>-BTBP are still relatively  
 slow, so the addition of a phase-transfer catalyst is necessary  
 [e.g., *N,N'*-dimethyl-*N,N'*-dioctylethylethoxymalonamide  
 (DMDOHEMA)] if this extractant is to be used for large-  
 scale partitioning.<sup>19</sup> In an attempt to improve the kinetics of  
 extraction with these tetradentate N-donor extractants, greater  
 conformational rigidity was enforced in the ligand backbone  
 with the synthesis of 2,9-bis(5,5,8,8-tetramethyl-5,6,7,8-tetrahy-  
 dro-1,2,4-benzotriazin-3-yl)-1,10-phenanthroline (CyMe<sub>4</sub>-  
 BTPhen; Figure 1).<sup>20</sup> This rigid ligand displays very high  
 separation factors for  $\text{Am}^{3+}$  over  $\text{Eu}^{3+}$  (up to 400) with  
 significantly faster kinetics of extraction compared to those  
 found for CyMe<sub>4</sub>-BTBP, thereby eliminating the need for a  
 phase-transfer catalyst.<sup>20</sup> These high separation factors even at  
 low acidities for the aqueous phase may prove problematic  
 during back-extractions,<sup>7</sup> but the use of alternative diluents has  
 shown that efficient back-extractions may be achievable when  
 using the CyMe<sub>4</sub>-BTPhen extractant.<sup>20</sup>

An alternative concept being considered in Europe for the  
 recovery of actinides from SNF is the GANEX (Group  
 ActiNide EXtraction) process, which is proposed to consist 164

165 of two cycles.<sup>16,21,22</sup> Most of the uranium is removed in the first  
 166 cycle, while the second cycle recovers all of the remaining  
 167 actinides, mainly the transuranics neptunium through curium,  
 168 concurrently in varying oxidation states (III–VI) from the  
 169 fission products found in spent fuel, including the lanthanides.  
 170 The GANEX process is aimed for generation IV nuclear fuel  
 171 cycles, where plutonium is likely to exist in higher  
 172 concentrations during partitioning processes compared to  
 173 those found in the processing of SNF in current cycles.<sup>21</sup>  
 174 The major novelty with GANEX compared to most other more  
 175 technologically mature separation processes is that the  
 176 plutonium is routed with the minor actinides rather than with  
 177 the majority of the uranium. The separation of Am<sup>3+</sup> and Cm<sup>3+</sup>  
 178 from the lanthanide ions in a SANEX process is already  
 179 considered extremely challenging, so performing the same  
 180 separation in addition to partitioning neptunium, plutonium,  
 181 and any remaining uranium from all of the fission products in  
 182 the second stage of the GANEX process is even more difficult.  
 183 A single extractant in the organic phase is unlikely to achieve  
 184 the group separation of multiple actinides in variable oxidation  
 185 states with appropriate efficiencies. Consequently, the perform-  
 186 ance of multiple extractants in the organic phase, typically  
 187 already established from other separation processes, has been  
 188 explored for use in a GANEX process.<sup>16,21,22</sup> A number of  
 189 different extractant combinations have been shown to have  
 190 potential including *N,N,N',N'*-tetraoctyldiglycolamide  
 191 (TODGA; used in DIAMEX) with DMDOHEMA, TODGA  
 192 with TBP, and CyMe<sub>4</sub>-BTBP with TBP.<sup>16,21,22</sup>  
 193 The N-donor extractants CyMe<sub>4</sub>-BTPhen and CyMe<sub>4</sub>-BTBP  
 194 have already demonstrated potential as extractants for  
 195 partitioning SNF mixtures, in particular the separation of  
 196 minor actinides from the lanthanides.<sup>7,18–20</sup> However, the  
 197 mode of action of these ligands with these metal ions in  
 198 extraction conditions has not been definitively established.  
 199 Here, we have produced numerous Ln<sup>3+</sup> complexes across the  
 200 lanthanide series with both CyMe<sub>4</sub>-BTPhen and CyMe<sub>4</sub>-BTBP  
 201 ligands using a direct synthetic approach. These complexes  
 202 have been fully characterized in both solution and solid states  
 203 using multiple techniques including electronic absorption  
 204 spectroscopy, luminescence spectroscopy, and single-crystal  
 205 X-ray diffraction (XRD). We have then used X-ray absorption  
 206 spectroscopy (XAS) to probe the lanthanide (europium and  
 207 terbium) species, which have been extracted into the organic  
 208 phase using conditions similar to those proposed for SANEX  
 209 and GANEX separation processes that use CyMe<sub>4</sub>-BTPhen and  
 210 CyMe<sub>4</sub>-BTBP. The extended X-ray absorption fine structure  
 211 (EXAFS) of the Ln L<sub>III</sub>-edge XAS spectra obtained from each  
 212 of these systems has been fitted to structural models established  
 213 by characterization of the directly synthesized Ln<sup>3+</sup> complexes  
 214 with these N-donor extractants, thus providing definitive  
 215 evidence for Ln<sup>3+</sup> speciation in the bulk organic phase during  
 216 extraction processes.

## 217 ■ RESULTS AND DISCUSSION

218 **Synthesis.** Ln<sup>III</sup> complexes of the extractant CyMe<sub>4</sub>-  
 219 BTPhen (see Table 1 for the list) were readily synthesized by  
 220 the addition of Ln(NO<sub>3</sub>)<sub>3</sub> (Ln = Pr, Eu, Tb, Yb) in acetonitrile  
 221 to 1 mol equiv of CyMe<sub>4</sub>-BTPhen in dichloromethane (DCM).  
 222 The reaction solution was allowed to evaporate to dryness,  
 223 leaving a powder that could be crystallized from a mixture of  
 224 CH<sub>3</sub>CN, DCM, and ethanol in a volume ratio of ~2:2:1, where  
 225 CH<sub>3</sub>CN readily dissolves the complex, DCM acts to reduce the  
 226 solubility of the complex in solution, and ethanol improves the

**Table 1. List of Synthesized Complexes**

formula	compound number
[Pr(CyMe <sub>4</sub> -BTPhen) <sub>2</sub> (NO <sub>3</sub> )](NO <sub>3</sub> ) <sub>2</sub> ·10H <sub>2</sub> O	1
[Pr(CyMe <sub>4</sub> -BTPhen) <sub>2</sub> (NO <sub>3</sub> )] [Pr(NO <sub>3</sub> ) <sub>5</sub> ] <sup>2-</sup> ·1.63EtOH·0.75H <sub>2</sub> O	2
[Eu(CyMe <sub>4</sub> -BTPhen) <sub>2</sub> (H <sub>2</sub> O)](NO <sub>3</sub> ) <sub>3</sub> ·9H <sub>2</sub> O	3
[Tb(CyMe <sub>4</sub> -BTPhen) <sub>2</sub> (H <sub>2</sub> O)](NO <sub>3</sub> ) <sub>3</sub> ·9H <sub>2</sub> O	4
[Yb(CyMe <sub>4</sub> -BTPhen) <sub>2</sub> (H <sub>2</sub> O)](NO <sub>3</sub> ) <sub>3</sub> ·9H <sub>2</sub> O	5
[Pr(CyMe <sub>4</sub> -BTBP) <sub>2</sub> (NO <sub>3</sub> )](NO <sub>3</sub> ) <sub>2</sub> ·4EtOH·H <sub>2</sub> O	6
[Pr(CyMe <sub>4</sub> -BTBP) <sub>2</sub> (NO <sub>3</sub> ) <sub>2</sub> ][Pr(NO <sub>3</sub> ) <sub>6</sub> ](NO <sub>3</sub> ) <sub>3</sub> ·6CH <sub>3</sub> CN	7
[Eu(CyMe <sub>4</sub> -BTBP) <sub>2</sub> (NO <sub>3</sub> )](NO <sub>3</sub> ) <sub>2</sub> ·4EtOH·2H <sub>2</sub> O	8
[Eu(CyMe <sub>4</sub> -BTBP)(NO <sub>3</sub> ) <sub>3</sub> ] <sup>2-</sup> ·toluene	9
[Tb(CyMe <sub>4</sub> -BTBP) <sub>2</sub> (H <sub>2</sub> O)](NO <sub>3</sub> ) <sub>3</sub> ·4EtOH	10

227 miscibility of the solvent mixture. In all examples, yellow  
 228 crystals were obtained. Elemental analysis, single-crystal XRD  
 229 (see the Solid-State Structure section), and electrospray  
 230 ionization mass spectrometry (ESI-MS, positive ion) indicated  
 231 that, in the majority of cases, complex cations of stoichiometry  
 232 1:2 Ln<sup>3+</sup>/CyMe<sub>4</sub>-BTPhen with nitrate counterions were  
 233 obtained even though the syntheses were conducted with  
 234 equimolar amounts of Ln(NO<sub>3</sub>)<sub>3</sub> and CyMe<sub>4</sub>-BTPhen. The  
 235 only exception was found during the synthesis of the Pr<sup>3+</sup>  
 236 complex of CyMe<sub>4</sub>-BTPhen, where the major product consisted  
 237 of a 1:2 Pr/CyMe<sub>4</sub>-BTPhen complex cation but with a  
 238 [Pr(NO<sub>3</sub>)<sub>5</sub>]<sup>2-</sup> counterion present per cationic unit. The initial  
 239 crystallization of this mixture led to isolation of a small amount  
 240 of this cationic species with only nitrate present as counterions,  
 241 as determined by XRD (see the Solid-State Structure section).  
 242 The structural determinations show that the Ln<sup>3+</sup> coordination  
 243 sphere is completed by a single nitrate anion for the Pr<sup>3+</sup>  
 244 complexes (1 and 2), while for the Eu<sup>3+</sup>, Tb<sup>3+</sup>, and Yb<sup>3+</sup>  
 245 complexes (3–5), a single molecule of water completes the  
 246 coordination sphere (see the Solid-State Structure section).  
 247 However, ESI-MS spectrometry of all the studied Ln<sup>3+</sup>  
 248 complexes with CyMe<sub>4</sub>-BTPhen from a methanol (MeOH)  
 249 solution indicates that a nitrate ion is coordinated, and there  
 250 was no evidence to suggest that a water molecule was present in  
 251 the coordination sphere.

252 The synthesis of Ln<sup>3+</sup> complexes (Ln = Pr, Eu, Tb) of  
 253 CyMe<sub>4</sub>-BTBP (see Table 1 for the list) was also attempted by  
 254 adding a DCM solution of the ligand to 0.5 equiv of Ln(NO<sub>3</sub>)<sub>3</sub>  
 255 in MeOH. The powder obtained upon evaporation of the  
 256 reaction mixture was best crystallized by slow evaporation from  
 257 a 1:1:1:1 by volume mixture of toluene, isopropyl alcohol,  
 258 ethanol, and DCM. The alcohols dissolve the complexes  
 259 reasonably well, while the use of toluene and DCM reduces the  
 260 solubility of the complexes, assists in controlling the rate of  
 261 evaporation, and provides reasonable miscibility in these  
 262 solvent mixtures. Characterization of the bulk crystallized  
 263 material obtained from all of the attempted Ln<sup>3+</sup> complexations  
 264 of CyMe<sub>4</sub>-BTBP indicated that a mixture of products was  
 265 present, which is likely to be due to the formation of products  
 266 with different combinations of Ln<sup>3+</sup>/CyMe<sub>4</sub>-BTBP ratios and  
 267 anionic molecular ions (i.e., NO<sub>3</sub><sup>-</sup>, [Ln(NO<sub>3</sub>)<sub>6</sub>]<sup>3-</sup>, [Ln-  
 268 (NO<sub>3</sub>)<sub>5</sub>]<sup>2-</sup>). However, the selection of individual crystals  
 269 obtained from these reactions was able to afford the structural  
 270 determination of a number of products by XRD. The vast  
 271 majority of these structures indicated complex cations of 1:2  
 272 Ln<sup>3+</sup>/CyMe<sub>4</sub>-BTBP stoichiometry (6–8 and 10) with nitrates  
 273 (6–8 and 10) and metallonitrates (7) present as counterions.  
 274 The first structures of Ln-BTBP complexes to be isolated were 274

275 with the ligand 6,6'-bis(5,6-diethyl-1,2,4-triazin-3-yl)-2,2'-bipyridine (C2-BTBP), and these had a single C2-BTBP molecule  
 276 coordinated to the  $\text{Ln}^{3+}$  ion.<sup>23</sup> It was noted that in solution  
 277 both 1:1 and 1:2  $\text{Ln}^{3+}/\text{C2-BTBP}$  complexes were observed.<sup>23</sup>  
 278 More recently, crystals of  $[\text{Eu}(\text{CyMe}_4\text{-BTBP})_2(\text{NO}_3)]^{2+}$  with a  
 279 metallonitrate counterion and the charge-neutral species  
 280  $[\text{Eu}(\text{CyMe}_4\text{-BTBP})(\text{NO}_3)_3]$  were isolated by slow evaporation  
 281 from a mixture of DCM and  $\text{CH}_3\text{CN}$ .<sup>24</sup> Our attempts to form  
 282 the  $\text{Eu}^{3+}$  complex of  $\text{CyMe}_4\text{-BTBP}$  produced a 1:1  $\text{Eu}^{3+}/$   
 283  $\text{CyMe}_4\text{-BTBP}$  molecular species with a toluene molecule  
 284 present as a solvent of crystallization (9) in addition to the  
 285 1:2  $\text{Eu}^{3+}/\text{CyMe}_4\text{-BTBP}$  complex cation containing species but  
 286 with only nitrate counterions present in the lattice. The  $\text{Pr}^{3+}$   
 287 and  $\text{Eu}^{3+}$  complexes isolated in the solid state (6–9) have one  
 288 or more nitrate ions completing the coordination sphere, while  
 289 only the  $\text{Tb}^{3+}$  complex of  $\text{CyMe}_4\text{-BTBP}$  has a water molecule in  
 290 its coordination environment. The ESI-MS spectra of all of the  
 291  $\text{CyMe}_4\text{-BTBP}$  complexes obtained from MeOH indicated that  
 292 the only intact molecular species present was  $[\text{Ln}(\text{CyMe}_4\text{-}$   
 293  $\text{BTBP})_2(\text{NO}_3)]^{2+}$ . The ESI-MS spectra of the  $\text{CyMe}_4\text{-BTBP}$   
 294 complexes provide comparable results and are in agreement  
 295 with similar ESI-MS studies previously performed on extracted  
 296 solutions of  $\text{Eu}^{3+}$  with BTBP extractants.<sup>25</sup> This suggests that  
 297 the 1:2:1  $\text{Ln}^{3+}/\text{CyMe}_4\text{-BTBP}/\text{NO}_3^-$  complex is dominant in  
 298 solution, while other compositions were only present in  
 299 solution in minor quantities, if at all.

301 **Solution Spectroscopy.** The UV–visible absorption  
 302 spectra of complexes 2–4, isolated in a pure bulk form,  
 303 dissolved in MeOH are dominated by charge-transfer  
 304 transitions in the UV region of the spectra (see the Supporting  
 305 Information). These transitions are most likely due to  $\pi-\pi^*$   
 306 transitions from the aromatic nature of the  $\text{CyMe}_4\text{-BTBP}$   
 307 ligand. A clear difference in the spectral profile is observed  
 308 between the free  $\text{CyMe}_4\text{-BTBP}$  ligand and  $\text{Ln}^{3+}$  complexes,  
 309 indicating that the electronic structure of the  $\text{CyMe}_4\text{-BTBP}$   
 310 molecule is perturbed upon  $\text{Ln}^{\text{III}}$  coordination. Essentially no  
 311 difference is observed between the spectroscopic profiles for 2–  
 312 4, indicating that there is little or no influence by the type of  
 313 coordinating lanthanide ion on the electronic structure of the  
 314  $\text{CyMe}_4\text{-BTBP}$  ligand. The limited solubility of these  
 315 complexes in most common solvents precluded the study of  
 316 the typically weakly absorbing  $f-f$  transitions of the lanthanides  
 317 in 1-cm-path-length cells.

318 Titrations of  $\text{CyMe}_4\text{-BTBP}$  and  $\text{CyMe}_4\text{-BTBP}$  with the  
 319 lanthanide ions,  $\text{Pr}^{3+}$ ,  $\text{Eu}^{3+}$ , and  $\text{Tb}^{3+}$  in MeOH were performed  
 320 to study the lanthanide speciation behavior of these extractant  
 321 molecules, in particular the equilibrium between 1:1 and 1:2  
 322  $\text{Ln}^{3+}/\text{L}_{\text{N}_4\text{-donor}}$  species. The titrations of  $\text{CyMe}_4\text{-BTBP}$  with  
 323 each of the lanthanides studied show that there is essentially no  
 324 difference in the titration profiles with different lanthanide ions  
 325 (see Figure 2 for  $\text{Pr}^{3+}$  and Supporting Information). Sharp  
 326 decreases in the intensity of the absorption maxima for free  $\text{CyMe}_4\text{-BTBP}$   
 327 at 261 and 295 nm with the addition of up to 0.5  
 328 equiv of  $\text{Ln}(\text{NO}_3)_3$  are observed. The absorption maximum at  
 329 261 nm also shifts to  $\sim 266$  nm with the addition of  $\text{Ln}(\text{NO}_3)_3$ .  
 330 Isosbestic points are observed at 229 and 279 nm. Further  
 331 additions of  $\text{Ln}(\text{NO}_3)_3$ , up to 3 equiv, result in a subtle decrease  
 332 in the absorption intensity for most of the spectrum but with  
 333 no changes in the shape of the spectral profile. This indicates  
 334 that the 1:2  $\text{Ln}^{3+}/\text{CyMe}_4\text{-BTBP}$  complex forms with the  
 335 initial addition of  $\text{Ln}(\text{NO}_3)_3$ , as expected.<sup>23,26</sup> The subtle  
 336 changes in the spectra when more than 0.5 equiv of  $\text{Ln}(\text{NO}_3)_3$

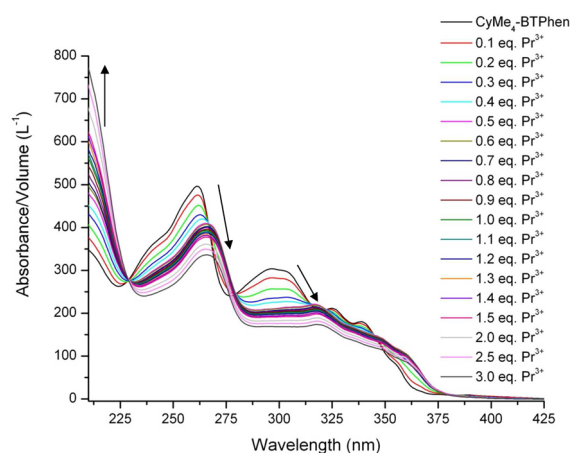


Figure 2. UV–visible absorption spectroscopic titration of  $\text{CyMe}_4\text{-BTPhen}$  with  $\text{Pr}(\text{NO}_3)_3$  in MeOH (initial conditions,  $[\text{CyMe}_4\text{-BTPhen}] = 2.0 \times 10^{-5}$  M, volume = 2.0 mL; titrant conditions,  $[\text{Pr}(\text{NO}_3)_3] = 4.0 \times 10^{-4}$  M).

is present in solution are most likely explained by an  
 equilibrium being established between 1:1 and 1:2  $\text{Ln}^{3+}/$   
 $\text{CyMe}_4\text{-BTPhen}$  species, where more 1:1 complex is likely to  
 form with increasing additions of  $\text{Ln}(\text{NO}_3)_3$ . Similar behavior is  
 observed for the titrations of  $\text{CyMe}_4\text{-BTBP}$  with  $\text{Ln}(\text{NO}_3)_3$   
 (see Figure 3 for  $\text{Eu}^{3+}$  and Supporting Information).

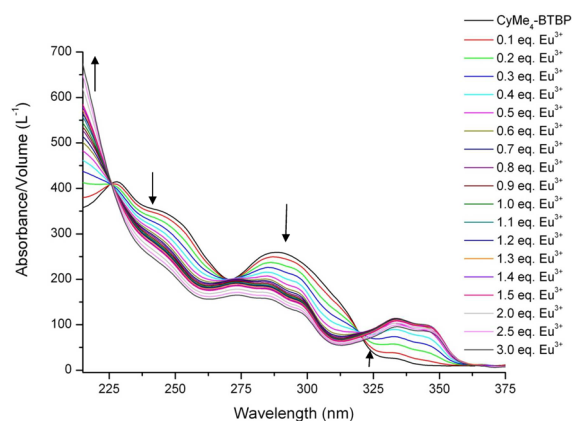


Figure 3. UV–visible absorption spectroscopic titration of  $\text{CyMe}_4\text{-BTBP}$  with  $\text{Eu}(\text{NO}_3)_3$  in MeOH (initial conditions,  $[\text{CyMe}_4\text{-BTBP}] = 2.0 \times 10^{-5}$  M, volume = 2.0 mL; titrant conditions,  $[\text{Eu}(\text{NO}_3)_3] = 4.0 \times 10^{-4}$  M).

Absorption maxima at 228 and 289 nm sharply decrease in  
 intensity with the initial addition of  $\text{Ln}(\text{NO}_3)_3$  up to 0.5 equiv.  
 Two absorption maxima are seen to emerge at 334 and 346 nm  
 with the initial addition of  $\text{Ln}(\text{NO}_3)_3$ . Further additions of  
 $\text{Ln}(\text{NO}_3)_3$  also result in a subtle decrease in the absorption  
 intensity for most of the spectrum. Therefore, it can be  
 deduced that the 1:2  $\text{Ln}^{3+}/\text{CyMe}_4\text{-BTBP}$  complex is probably  
 most favored to form, but the 1:1 species can be forced to form  
 in solution with excess  $\text{Ln}^{3+}$  ion present. Similar results have  
 been previously observed for  $\text{Ln}^{3+}$  complexation behavior with  
 analogous BTBP ligands.

The overall stability constants for both 1:1 and 1:2  $\text{Ln}^{3+}/$   
 $\text{CyMe}_4\text{-BTBP}$ – $\text{CyMe}_4\text{-BTBP}$  species were determined by  
 fitting the appropriate spectrophotometric titration data (Table  
 2). These fits confirm that the formation of both  $\text{ML}$  and  $\text{ML}_2$   
 (where L is the N-donor ligand) species does occur over the

**Table 2. Fitted Metal–Ligand Overall Stability Constants Determined from UV–Visible Spectroscopic Data Using Hyperquad<sup>28</sup> ( $I = 0$  M in MeOH;  $T = 25$  °C)**

N-donor ligand	Ln <sup>3+</sup>	overall stability constant ( $\log \beta_{ML}$ )				$\sigma^b$
		$\log \beta_{11}$	standard deviation <sup>a</sup>	$\log \beta_{12}$	standard deviation <sup>a</sup>	
CyMe <sub>4</sub> -BTPPhen	Pr <sup>3+</sup>	4.7	0.5	11.8	0.1	0.0032
	Eu <sup>3+</sup>	7.9	0.5	15.6	1.0	0.0028
	Tb <sup>3+</sup>	8.1	0.5	13.2	0.5	0.011
CyMe <sub>4</sub> -BTBP	La <sup>3+</sup>	4.4 <sup>c</sup>	0.2 <sup>c</sup>	8.8 <sup>c</sup>	0.1 <sup>c</sup>	
	Pr <sup>3+</sup>	10.9	0.7	18.9	1.1	0.0042
	Eu <sup>3+</sup>	9.5	0.6	16.9	1.1	0.0067
		6.5 <sup>c</sup>	0.2 <sup>c</sup>	11.9 <sup>c</sup>	0.5 <sup>c</sup>	
	Tb <sup>3+</sup>	8.8	0.2	15.9	0.4	0.0037
	Yb <sup>3+</sup>	5.9 <sup>c</sup>	0.1 <sup>c</sup>			

<sup>a</sup>Standard deviations determined by the fitting process. <sup>b</sup>Goodness-of-fit parameter. <sup>c</sup>Reference 27 ( $I = 0.01$  M Et<sub>4</sub>NNO<sub>3</sub>;  $T = 25$  °C; in MeOH; determined by UV–visible absorption spectroscopy).

conditions used in these titrations, as has been observed previously in similar titrations of CyMe<sub>4</sub>-BTBP with Eu<sup>3+</sup>.<sup>27</sup> The speciation plots corresponding to the titrations with CyMe<sub>4</sub>-BTBP (see the Supporting Information) show the initial emergence of the ML<sub>2</sub> species when less than 0.5 mol equiv of lanthanide is present (relative to L), with further additions of lanthanide showing the increasing formation of the ML species. The magnitude of the lanthanide stability constants for the CyMe<sub>4</sub>-BTBP species indicates the greatest affinity for the mid-lanthanides with lower stability constants obtained for the lanthanides at either end of the series, which is in agreement with previous work and the corresponding distribution ratios for Ln<sup>3+</sup> extractions using CyMe<sub>4</sub>-BTBP and DMDOHEMA into *n*-octanol.<sup>12,27</sup> The speciation plots for the CyMe<sub>4</sub>-BTPPhen titrations (see the Supporting Information) indicate behavior different from that observed for CyMe<sub>4</sub>-BTBP. For Pr<sup>3+</sup>, the 1:2 Ln/CyMe<sub>4</sub>-BTPPhen species is favored to form, compared to the 1:1 M/L species even at relatively high metal concentrations due to a highly positive cooperative effect for the formation of the ML<sub>2</sub> species. However, this strong cooperative effect diminishes substantially with progress along the lanthanide series where the ML species is predominantly favored for Tb<sup>3+</sup> even at reasonably low metal concentrations. The stability constants for 1:1 Ln/CyMe<sub>4</sub>-BTPPhen increases as the lanthanide series is traversed. The differences observed between the lanthanide stability behaviors for complexes of CyMe<sub>4</sub>-BTBP and CyMe<sub>4</sub>-BTPPhen are most likely due to the lack of flexibility in the BTPPhen backbone, resulting in the greater likelihood of a mismatch between the lanthanide ionic radius and the CyMe<sub>4</sub>-BTPPhen binding cavity as the lanthanide series is traversed.

The absorption spectroscopic profiles showed little difference between the light and heavy lanthanides, but XRD studies (see the Solid-State Structure section) indicate that the heavy lanthanides in the 1:2 Ln<sup>3+</sup>/CyMe<sub>4</sub>-BTPPhen–CyMe<sub>4</sub>-BTBP complexes prefer to have their coordination sphere completed by water, whereas the lighter lanthanide complexes generally prefer to have nitrate in their coordination environment, a consequence of the lanthanide contraction. This is commonly observed in a series of lanthanide complexes of a given multidentate ligand.<sup>29</sup> Luminescence studies were therefore undertaken in an attempt to assess the involvement of nitrate

and water in the coordination sphere of these lanthanide species, as has been performed previously to investigate the coordination behavior of other extractant molecules.<sup>30</sup> Excitation and emission spectra of the Eu<sup>3+</sup> and Tb<sup>3+</sup> complexes with CyMe<sub>4</sub>-BTPPhen and CyMe<sub>4</sub>-BTBP are displayed in Figure 4 and in the Supporting Information. Excitation into the

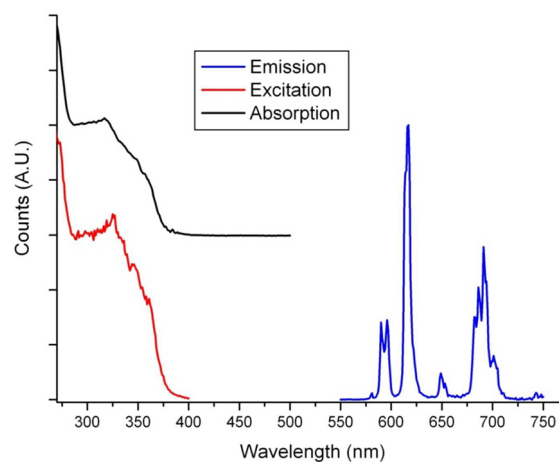


**Figure 4.** Emission (following excitation at 320 nm), excitation (monitoring emission at 616 nm), and absorption spectra of [Eu(CyMe<sub>4</sub>-BTPPhen)<sub>2</sub>(X)]<sup>n+</sup> in MeOH ( $X = \text{H}_2\text{O}/\text{NO}_3^-$ ;  $n = 3$  and 2).

intraligand absorption bands (280–330 nm) of the Eu<sup>3+</sup> and Tb<sup>3+</sup> complexes produced characteristic f-centered emission spectra with resolvable bands due to the <sup>5</sup>D<sub>0</sub> to <sup>7</sup>F<sub>J</sub> and <sup>5</sup>D<sub>4</sub> to <sup>7</sup>F<sub>J</sub> ( $J = 0–6$ ) transitions, respectively. The emission spectrum of the Eu<sup>3+</sup> complexes are dominated by the electric-dipole-allowed  $\Delta J = 2$  transition, which is hypersensitive to the site symmetry. The absence of a hyperfine structure in this band indicates that the complexes exist as a single emissive species on the experimental time scale.<sup>31</sup> The emission profiles for the Eu<sup>3+</sup> complexes are similar to those observed with other BTBP ligands, but in our examples, the splitting of the <sup>5</sup>D<sub>0</sub> to <sup>7</sup>F<sub>2</sub> transition at ~617 nm upon complexation with the N-donor ligands is not resolved, which has been observed previously in some examples.<sup>24,32</sup> The respective excitation spectra recorded at the emission maxima (545 nm for Tb<sup>3+</sup> and 616 nm for Eu<sup>3+</sup>) display ligand-centered absorption bands that overlap well with the absorption spectra, indicating that sensitized emission is occurring in all of the systems under study.

In order to assess the inner coordination sphere of the complexes, lifetime data were recorded in MeOH and MeOH-*d*<sub>4</sub> following 320 nm excitation (e.g., see Figure 5) and the number of coordinated MeOH molecules determined according to Horrock's equation (eq 1)<sup>33</sup>

$$q_{\text{bound MeOH}} = A \left[ \left( \frac{1}{\tau_{\text{MeOH}}} \right) - \left( \frac{1}{\tau_{\text{CD}_3\text{OD}}} \right) \right] \quad (1)$$

where  $A$  is a proportionality constant;  $A = 2.1$  ms for Eu<sup>3+</sup> and  $A = 8.4$  ms for Tb<sup>3+</sup>.

For solutions of Eu<sup>3+</sup> and CyMe<sub>4</sub>-BTPPhen in a 2:1 molar ratio, this gave a  $q$  value of 0.3; an identical  $q$  value was obtained for the analogous complex with CyMe<sub>4</sub>-BTBP of 0.3 (Table 3). This strongly suggests that the first coordination sphere of the complexes is completed by ligation of nitrate

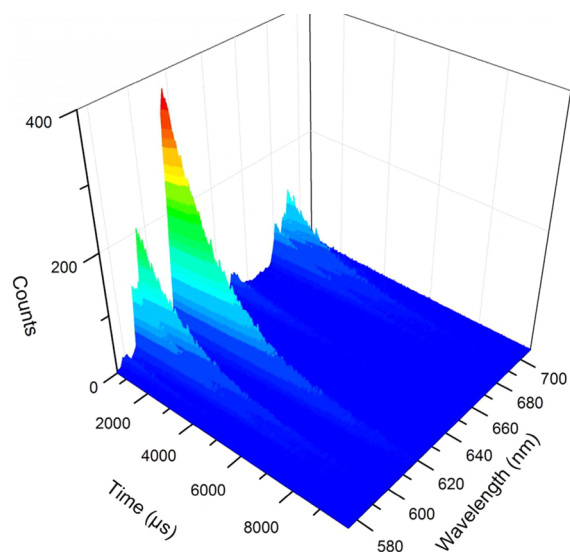


**Figure 5.** Time-resolved emission spectrum of  $[\text{Eu}(\text{CyMe}_4\text{-BTPhen})_2(\text{X})]^{n+}$  in MeOH following excitation at 320 nm ( $\text{X} = \text{H}_2\text{O}/\text{NO}_3^-$ ;  $n = 3$  and  $2$ ).

**Table 3. Photophysical Properties of Solutions of  $\text{Ln}(\text{NO}_3)_3$  with Tetra-N-Donor Ligands in a 1:2 Molar Ratio at 298 K<sup>a</sup>**

complex	$\lambda_{\text{em}}$ (nm)	$\tau_{\text{MeOH}}$ (ms)	$\tau_{\text{MeOD}}$ (ms)	$q_{\text{MeOH}}$
$[\text{Eu}(\text{BTBP})_2(\text{X})]^{n+}$	617	1.94	2.61	0.3
$[\text{Eu}(\text{BTPhen})_2(\text{X})]^{n+}$	617	1.49	1.87	0.3

<sup>a</sup>All lifetimes were recorded by TCSPC at 320 nm excitation using a 5 W xenon flashlamp and are subject to a  $\pm 10\%$  error. Identical data within error were obtained for 1:3 and 1:5 solutions of  $\text{Eu}^{3+}/\text{L}_{\text{N}_4\text{-donor}}$  and the crystalline complexes **3** and **8**.

438 anions rather than exchangeable solvent molecules, and there  
439 may be a minor species that exists, with either water or MeOH  
440 occupying this coordination site for these  $\text{Eu}^{3+}$  complexes.  
441 Because the emissive quantum yield of a solvated species would  
442 be much lower, the contribution to the initial emission intensity  
443 will be low, perhaps precluding observation of a second species  
444 in solution, and/or the rate of solvent and nitrate anion  
445 exchange is much faster than the luminescence time scale, so a  
446 noninteger value of  $q$  is determined. Similar data were obtained  
447 for 1:3 and 1:5 molar ratios of  $\text{Eu}^{3+}$  with both  $\text{N}_4$ -donor ligands  
448 and the isolated complexes **3** and **8**, suggesting that the 1:2  
449  $\text{Ln}^{3+}/\text{L}_{\text{N}_4\text{-donor}}$  complex is the only emissive species formed  
450 under these conditions.

451 In the case of the  $\text{Tb}^{3+}$  complexes of both ligands, excitation  
452 into the ligand absorption bands resulted in comparatively weak  
453 emission spectra. This is unsurprising given the estimated  
454 triplet energies of the ligands and the high-energy emissive  $^5\text{D}_4$   
455 excited state and suggests that back-energy transfer from the  
456  $\text{Tb}^{3+}$  excited-state manifold to the ligand triplet state is a  
457 competitive nonradiative decay process.<sup>34</sup> This is corroborated  
458 by the fact that the radiative lifetimes for the  $\text{Tb}^{3+}$  emission are  
459 extremely short; the kinetic traces could be satisfactorily fitted  
460 with two exponential functions, giving lifetime values of  
461 approximately 18 and 6  $\mu\text{s}$  (for solutions of BTBP in  
462 MeOH). Moreover, the kinetic traces recorded without a  
463 time gate and delay additionally exhibit a short-lived  
464 component of nanosecond order, which we attribute to  
465 ligand-centered emission.

**Solid-State Structure.** Single-crystal XRD studies of 466  
complexes of  $\text{Tb}^{3+}$ ,  $\text{Eu}^{3+}$ , and  $\text{Pr}^{3+}$  with ligands  $\text{CyMe}_4\text{-BTBP}$  467  
and  $\text{CyMe}_4\text{-BTPhen}$  were obtained (**1–4** and **6–10**, 468  
respectively). The complex of  $\text{Yb}^{3+}$  with  $\text{CyMe}_4\text{-BTPhen}$  was 469  
also studied (**5**). Complexes **3–5** are isostructural crystallizing 470  
in the orthorhombic space group  $Fdd2$ . Plots of these structures 471  
are displayed in Figures 6–11 (complexes **1**, **3**, **6**, and **8–10**) 472 f6 – f11

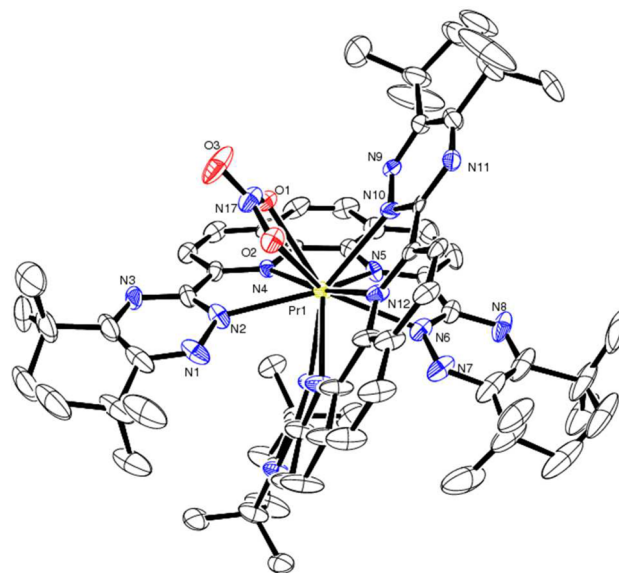


**Figure 6.** ORTEP plot of the complex cation of **1**, with crystallographic numbering (H atoms omitted). Probability ellipsoids of 50% displayed.

and the Supporting Information (complexes **2**, **4**, **5**, and **7**) with 473  
crystal data given in Tables 4 and 5. In the vast majority of 474 445  
cases (**1–8** and **10**), two of the N-donor ligands (either 475  
 $\text{CyMe}_4\text{-BTBP}$  or  $\text{CyMe}_4\text{-BTPhen}$ ) were found to coordinate to 476  
the metal center occupying four coordination sites each, with 477  
another ligand (water or nitrate) occupying a cavity between 478

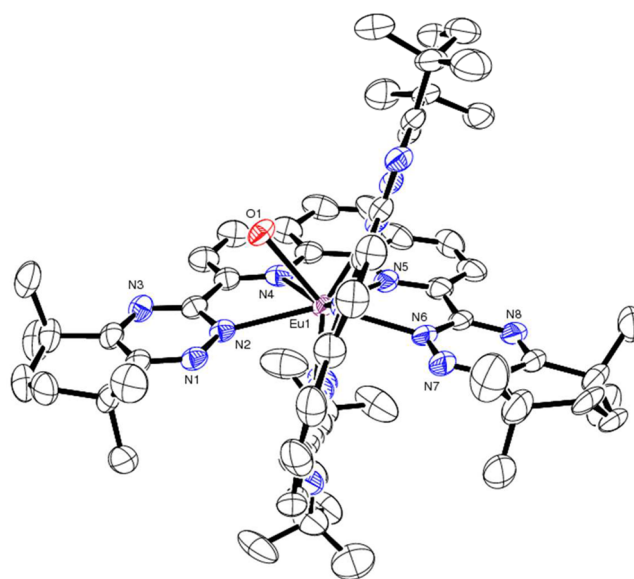


**Figure 7.** ORTEP plot of the complex cation of **3**, with crystallographic numbering (H atoms omitted). Probability ellipsoids of 50% displayed.

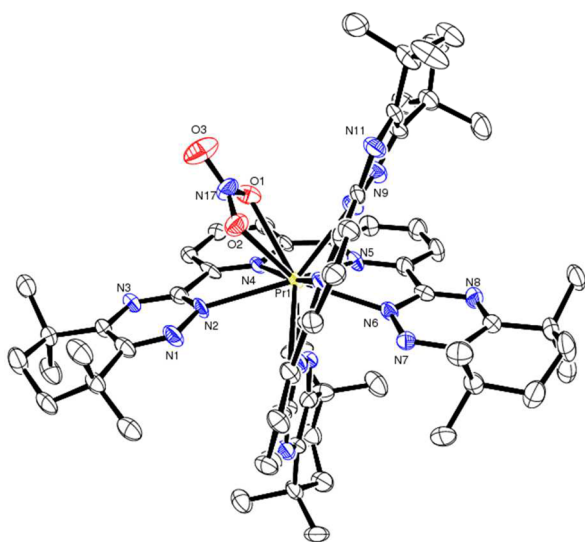


**Figure 8.** ORTEP plot of the complex cation of **6**, with crystallographic numbering (H atoms omitted). Probability ellipsoids of 50% displayed.

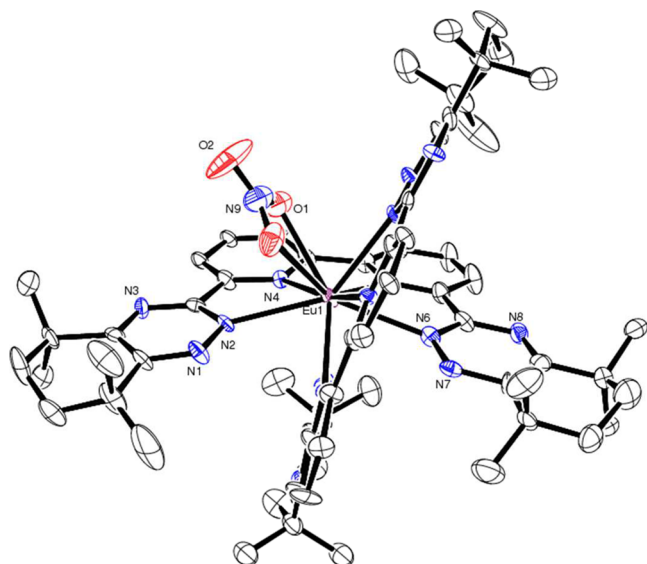


**Figure 9.** ORTEP plot of the complex cation of **8**, with crystallographic numbering (H atoms omitted). Probability ellipsoids of 50% displayed.

479 the two bound N-donor ligands, giving a distorted capped  
480 square-antiprismatic geometry about the  $\text{Ln}^{3+}$  center. This leads  
481 to a total coordination number of 9 for water-coordinated  
482 complexes (**3–5** and **10**) and 10 for the bidentate nitrate-  
483 coordinated complexes (**1**, **2**, and **6–8**).

484 For the  $\text{Ln}^{3+}$  complexes with  $\text{CyMe}_4\text{-BTPhen}$ , only 1:2  $\text{Ln}^{3+}/$   
485  $\text{L}_{\text{N-donor}}$  coordination stoichiometries have been isolated and  
486 structurally characterized in the solid state. The nitrate ion is  
487 found to occupy the remaining coordination sites in the  $\text{Pr}^{3+}$   
488 complexes isolated, while a single water molecule completes the  
489 coordination sphere for the  $\text{CyMe}_4\text{-BTPhen}$  complexes of the  
490 heavier  $\text{Ln}^{3+}$  ions investigated in this study ( $\text{Eu}^{3+}$ ,  $\text{Tb}^{3+}$ , and  
491  $\text{Yb}^{3+}$  in **3–5**). This is likely to be due to a combined effect of  
492 the lanthanide contraction and the structural rigidity of the  
493  $\text{CyMe}_4\text{-BTPhen}$  ligand sterically hindering the remaining  
494 coordination sites in the more contracted structures of  $\text{Eu}^{3+}$ ,

$\text{Tb}^{3+}$ , and  $\text{Yb}^{3+}$  such that only water can access this binding  
495 cavity in these solid-state systems. However, previous work has  
496 shown that the 1:2 complex of  $\text{Eu}^{3+}/\text{CyMe}_4\text{-BTPhen}$  can be  
497 obtained with a nitrate ion completing the coordination sphere  
498 in the solid state where MeOH was used as the reaction  
499 solvent,<sup>20</sup> thus indicating that the position of the equilibrium  
500 between bound nitrate and bound water in these  $\text{Ln}^{3+}$   
501 complexes may be influenced by the choice of solvent. The  
502 nitrate-coordinated complexes form 2+ charged complex  
503 cations, while the water-coordinated complexes form tricationic  
504 complex cations, where charge balance is achieved with  
505 nonbinding nitrate anions in the crystal lattice (**1** and **3–5**)  
506 or with an anionic metallonitrate species (**2**). The previously  
507 obtained  $[\text{Eu}(\text{CyMe}_4\text{-BTPhen})_2(\text{NO}_3)]^{2+}$  solid-state complex  
508 was also charge-balanced with a pentanitratolanthanide anionic  
509 species.<sup>20</sup>

510 All of the M–N bond lengths in the  $\text{CyMe}_4\text{-BTPhen}$ -  
511 containing structures decrease as the lanthanide series is  
512 traversed from left to right (Table 6), as expected due to the  
513 lanthanide contraction. In all cases, the lanthanide ion sits  
514 outside of the plane of the N-donor ligand cavity. The out-of-  
515 plane displacement of the  $\text{Ln}^{3+}$  ion from the average plane  
516 defined by the four coordinating N atoms for each N-donor  
517 ligand follows a trend similar to that of the bond lengths by  
518 decreasing across the lanthanide series:  $\sim 0.80/0.71$ ,  $0.77/0.62$ ,  
519  $0.56$ ,  $0.55$ , and  $0.51$  Å for species **1–5**, respectively. The  
520 average M– $\text{N}_{\text{triazinyl}}$  bonds lengths are consistently longer than  
521 those for the M– $\text{N}_{\text{phen}}$  bonds in the  $\text{Eu}^{3+}$ ,  $\text{Tb}^{3+}$ , and  $\text{Yb}^{3+}$   
522 complexes (**3–5**). This may imply that a greater degree of  
523 interaction exists between the  $\text{Ln}^{3+}$  ion and the phenanthroline  
524 N-donor atoms than that with the triazinyl N-donor atoms.  
525 However, the same cannot be said for the structures of the  $\text{Pr}^{3+}$   
526 complexes obtained (**1** and **2**), where in some instances the  
527 M– $\text{N}_{\text{phen}}$  bond lengths are, in fact, longer than the M– $\text{N}_{\text{triazinyl}}$   
528 bond distances. The previously obtained structure of  $[\text{Eu}-$   
529  $(\text{CyMe}_4\text{-BTPhen})_2(\text{NO}_3)]^{2+}$  shows little difference between  
530 the  $\text{Eu}-\text{N}_{\text{triazinyl}}$  and  $\text{Eu}-\text{N}_{\text{phen}}$  bond distances.<sup>20</sup> Therefore, it is  
531 most likely the triazinyl groups that are restrained to be further  
532 away from the  $\text{Ln}^{3+}$  center relative to the phenanthroline  
533 backbone as the Ln center approaches the plane of the  $\text{CyMe}_4\text{-}$   
534  $\text{BTPhen}$  binding cavity, as this is only evident for the latter  
535 lanthanides. The  $\text{Ln}-\text{O}_{\text{water}}$  bond distances also decrease as the  
536 lanthanide series is traversed from left to right because of  
537 lanthanide contraction (Table 6). The  $\text{Pr}-\text{O}_{\text{nitrate}}$  bond  
538 distances for **1** and **2** [ $2.592(7)$  and  $2.544(7)$  Å for **1**;  
539  $2.581(5)$  and  $2.605(5)$  Å for **2**] are typical for  $\text{Pr}^{3+}$  complexes  
540 with coordinated nitrates ( $2.5\text{--}2.8$  Å).<sup>23,35,36</sup>

541 Where  $\text{CyMe}_4\text{-BTBP}$  is the ligand, both 1:1 (**9**) and 1:2  
542  $\text{Ln}^{3+}/\text{CyMe}_4\text{-BTBP}$  (**6–8** and **10**) coordination structures were  
543 isolated. Structures of metal complexes with  $\text{CyMe}_4\text{-BTBP}$  have  
544 only been previously obtained for  $\text{Eu}^{3+}$ ,  $\text{U}^{4+}$ , and  $\{\text{UO}_2\}^{2+}$ .<sup>36,37</sup>  
545 Previous studies of the complexation of  $\text{Eu}^{3+}$  with  $\text{CyMe}_4\text{-}$   
546  $\text{BTBP}$ , using a preparation similar to that described in this  
547 work, isolated structures consisting of the same 1:2 and 1:1  
548  $\text{Eu}^{3+}/\text{CyMe}_4\text{-BTBP}$  complexes found (structures **8** and **9**,  
549 respectively). However, these structures exhibit different crystal  
550 forms due to either different counterions or alternate solvent  
551 molecules of crystallization present in the lattices.<sup>24</sup> Further  
552 structural information has been obtained for  $\text{Ln}^{3+}$  complexes  
553 with  $\text{C2-BTBP}$ , where only 1:1  $\text{Ln}/\text{C2-BTBP}$  complexes were  
554 isolated, essentially for the entire lanthanide series.<sup>23</sup> The  
555 remaining coordination sites were occupied by three nitrate  
556 anions to give charge-neutral species.<sup>23</sup> The structure of the  
557

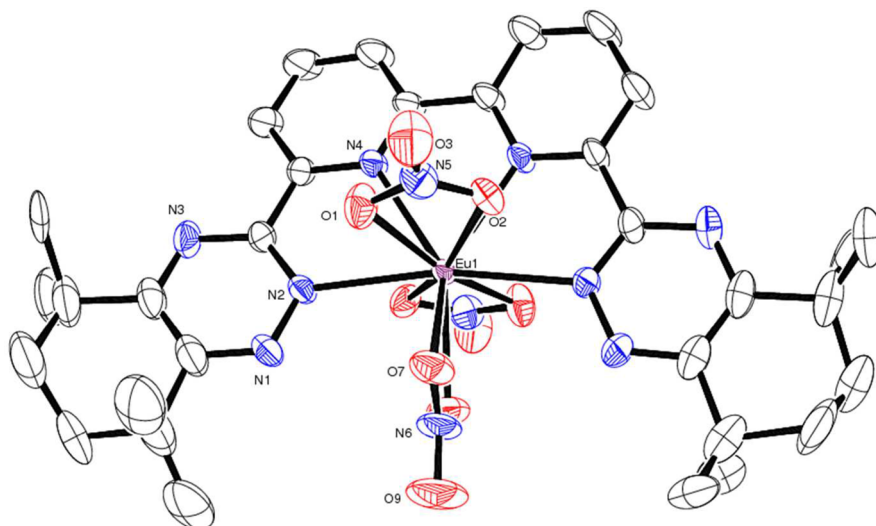


Figure 10. ORTEP plot of the complex molecule of **9**, with crystallographic numbering (H atoms omitted). Probability ellipsoids of 50% displayed.

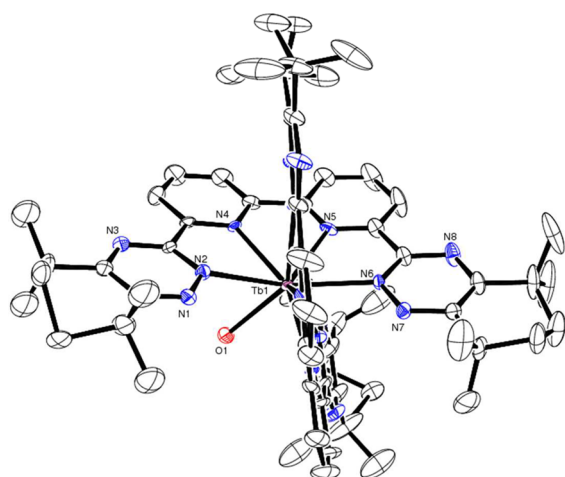


Figure 11. ORTEP plot of the complex cation of **10**, with crystallographic numbering (H atoms omitted). Probability ellipsoids of 50% displayed.

Eu<sup>3+</sup> complex, **9**, is analogous to the Ln<sup>3+</sup> complexes of C2-  
BTBP. For the cationic Ln<sup>3+</sup> complexes of CyMe<sub>4</sub>-BTBP,  
charge balance was achieved either with extra lattice nitrate  
anions (**6**, **8**, and **10**) or in combination with a  
hexanitratometallo anion (**7**). The two crystalline forms  
obtained from the complexation of Eu<sup>3+</sup> with CyMe<sub>4</sub>-BTBP  
offers further insight into the equilibrium between 1:1 and 1:2  
Ln/BTBP–BTPhen complex stoichiometries. Although it may  
be possible for both of these stoichiometries to be isolated, the  
vast majority of the structural evidence indicates that the  
lanthanides preferentially coordinate to two of these tetra N-  
donor ligands from this class of extractant molecules. In  
contrast to the CyMe<sub>4</sub>-BTPhen structures, metal-bound nitrate  
ions are observed with all CyMe<sub>4</sub>-BTBP species except Tb<sup>3+</sup>.  
This is presumably due to the greater flexibility afforded from  
the bipyridine, compared to the “locked” phenanthroline,  
permitting the sterically larger bidentate nitrate anion, relative  
to water, to bind to the Ln<sup>3+</sup> center.

For all of the complexes of CyMe<sub>4</sub>-BTBP (**6**–**10**), the Ln–N  
bond distances (Table 7) decrease as the lanthanide series is  
traversed from left to right, similar to the CyMe<sub>4</sub>-BTPhen and

C2-BTBP-containing structures.<sup>23</sup> The Ln–O<sub>nitrate</sub> bond  
lengths also clearly decrease across the series, demonstrating  
lanthanide contraction again. The 1:2 Ln<sup>3+</sup>/CyMe<sub>4</sub>-BTBP  
complexes bear further similarity to those of CyMe<sub>4</sub>-BTPhen  
with the Ln<sup>3+</sup> ion located outside of the average plane of the  
tetra-N-donor cavity and this displacement following the same  
trend as that of the bond lengths, decreasing across the series:  
~0.73/0.78, 0.72/0.76, 0.69, and 0.56 Å for **6**–**8** and **10**,  
respectively. However, the 1:1 Eu<sup>3+</sup>/CyMe<sub>4</sub>-BTBP complex (**9**)  
does effectively sit in the plane average plane of the four N-  
donor atoms (out-of-plane displacement ~0 Å). The  
coordination bond lengths and motifs observed in the  
structures of the 1:1 and 1:2 Eu<sup>3+</sup>/CyMe<sub>4</sub>-BTBP complexes  
(**8** and **9**) are similar to those observed for the structures  
obtained previously for the same complex molecules but in  
different crystal forms.<sup>24</sup> There is little difference observed  
in the Ln–N bond lengths between the 1:1 and 1:2 Ln<sup>3+</sup>/BTBP  
complex molecular species obtained here and elsewhere,<sup>23</sup>  
suggesting that if there are indeed any cooperative or  
destructive effects for 1:2 Ln<sup>3+</sup>/Cy-Me<sub>4</sub>-BTBP binding over  
the 1:1 Ln<sup>3+</sup>/Cy-Me<sub>4</sub>-BTBP complex, they do not significantly  
alter the N-donor coordination environment. In contrast to the  
CyMe<sub>4</sub>-BTPhen structures, there is no clearly identifiable trend  
between the M–N<sub>bipy</sub> and M–N<sub>triazinyl</sub> bond lengths for all of  
the CyMe<sub>4</sub>-BTBP complexes. This suggests that the greater  
flexibility of the bipyridyl group, relative to the phenanthroline  
group, allows minimal distinction between the triazinyl and  
bipyridyl N atoms when coordinated to a Ln<sup>3+</sup> ion.

**XAS of Lanthanide-Extracted Species.** XAS spectra were  
obtained for Eu<sup>3+</sup> and Tb<sup>3+</sup> species formed by extraction from  
an acidic aqueous phase into an organic phase containing an  
excess of either CyMe<sub>4</sub>-BTBP or CyMe<sub>4</sub>-BTPhen in cyclo-  
hexanone as a guide for speciation in a potential SANEX  
process. Studies were also performed for potential GANEX-like  
systems where the organic phase also included 30% TBP. XAS  
spectra were obtained for the crystallographically characterized  
solids [Eu(CyMe<sub>4</sub>-BTPhen)<sub>2</sub>(H<sub>2</sub>O)]<sup>3+</sup> (**3**) and [Tb(CyMe<sub>4</sub>-  
BTPhen)<sub>2</sub>(H<sub>2</sub>O)]<sup>3+</sup> (**4**) for comparative purposes. The spectra  
obtained show little difference between the extracted species  
with or without the presence of TBP (Figures 11 and 12 and  
the Supporting Information). This indicates that the presence  
of TBP does not influence lanthanide speciation when used in a

Table 4. Crystal Data for Complexes 1–5

	[Pr(CyMe <sub>4</sub> -BTPhen) <sub>2</sub> (NO <sub>3</sub> ) <sub>2</sub> ·10H <sub>2</sub> O (1)]	[Pr(CyMe <sub>4</sub> -BTPhen) <sub>2</sub> (NO <sub>3</sub> ) <sub>2</sub> ·1.63EtOH·0.75H <sub>2</sub> O (2)]	[Eu(CyMe <sub>4</sub> -BTPhen) <sub>2</sub> (H <sub>2</sub> O) <sub>2</sub> (NO <sub>3</sub> ) <sub>3</sub> ·9H <sub>2</sub> O (3)]	[Tb(CyMe <sub>4</sub> -BTPhen) <sub>2</sub> (H <sub>2</sub> O)(NO <sub>3</sub> ) <sub>3</sub> ·9H <sub>2</sub> O (4)]	[Yb(CyMe <sub>4</sub> -BTPhen) <sub>2</sub> (H <sub>2</sub> O) <sub>2</sub> (NO <sub>3</sub> ) <sub>3</sub> ·9H <sub>2</sub> O (5)]
formula	C <sub>68</sub> H <sub>96</sub> N <sub>19</sub> O <sub>19</sub> Pr	C <sub>71.25</sub> H <sub>87.25</sub> N <sub>22</sub> O <sub>20.38</sub> Pr <sub>2</sub>	C <sub>68</sub> H <sub>96</sub> N <sub>19</sub> O <sub>19</sub> Eu	C <sub>68</sub> H <sub>96</sub> N <sub>19</sub> O <sub>19</sub> Tb	C <sub>68</sub> H <sub>96</sub> N <sub>19</sub> O <sub>19</sub> Yb
<i>M</i>	1624.55	1859.70	1615.44	1642.56	1656.68
cryst syst	monoclinic	triclinic	orthorhombic	orthorhombic	orthorhombic
<i>a</i> (Å)	31.654(5)	13.716(5)	31.172(3)	31.3486(7)	31.3257(13)
<i>b</i> (Å)	26.271(5)	15.221(5)	38.128(3)	38.0261(9)	37.709(2)
<i>c</i> (Å)	19.501(5)	20.359(5)	14.8296(13)	14.8414(3)	14.8783(7)
<i>α</i> (deg)	90	107.225(5)	90	90	90
<i>β</i> (deg)	109.504(5)	99.422(5)	90	90	90
<i>γ</i> (deg)	90	97.083(5)	90	90	90
space group	<i>C2/c</i>	<i>P1</i>	<i>Fdd2</i>	<i>Fdd2</i>	<i>Fdd2</i>
<i>Z</i>	8	2	8	8	8
<i>T</i> (K)	100(2)	100(2)	100(2)	100(2)	100(2)
<i>μ</i> (mm <sup>-1</sup> )	0.719	1.309	0.782	0.870	1.135
reflms measd	20981	25422	32709	49820	8497
reflms obsd	6002	14178	8290	9044	5110
<i>R</i> <sub>1</sub> (obsd)	0.0551	0.0547	0.0512	0.0513	0.0658
<i>wR</i> <sub>2</sub> (all data)	0.1257	0.1393	0.1364	0.1423	0.1984

Table 5. Crystal Data for Complexes 6–10

	[Pr(CyMe <sub>4</sub> -BTBP) <sub>2</sub> (NO <sub>3</sub> ) <sub>2</sub> ·4EtOH·H <sub>2</sub> O (6)]	[Pr(CyMe <sub>4</sub> -BTBP) <sub>2</sub> (NO <sub>3</sub> ) <sub>2</sub> ][Pr(NO <sub>3</sub> ) <sub>6</sub> ](NO <sub>3</sub> ) <sub>6</sub> ·6CH <sub>3</sub> CN (7)]	[Eu(CyMe <sub>4</sub> -BTBP) <sub>2</sub> (NO <sub>3</sub> ) <sub>2</sub> (NO <sub>3</sub> ) <sub>2</sub> ·4EtOH·2H <sub>2</sub> O (8)]	[Eu(CyMe <sub>4</sub> -BTBP)(NO <sub>3</sub> ) <sub>3</sub> ·toluene (9)]	[Tb(CyMe <sub>4</sub> -BTBP) <sub>2</sub> (H <sub>2</sub> O) <sub>2</sub> (NO <sub>3</sub> ) <sub>3</sub> ·4EtOH (10)]
formula	C <sub>72</sub> H <sub>102</sub> N <sub>19</sub> O <sub>14</sub> Pr	C <sub>140</sub> H <sub>166</sub> N <sub>47</sub> O <sub>27</sub> Pr <sub>3</sub>	C <sub>72</sub> H <sub>104</sub> N <sub>19</sub> O <sub>15</sub> Eu	C <sub>46</sub> H <sub>54</sub> N <sub>11</sub> O <sub>9</sub> Eu	C <sub>72</sub> H <sub>102</sub> N <sub>19</sub> O <sub>14</sub> Tb
<i>M</i>	1598.64	3361.93	1627.70	1056.96	1614.63
cryst syst	monoclinic	monoclinic	orthorhombic	monoclinic	monoclinic
<i>a</i> (Å)	24.2790(7)	16.604(2)	16.4128(6)	26.385(2)	30.5621(7)
<i>b</i> (Å)	16.5467(4)	28.1161(19)	23.8916(6)	11.6674(11)	14.8217(4)
<i>c</i> (Å)	19.4601(5)	17.7385(14)	19.7838(6)	15.7469(14)	23.9083(6)
<i>α</i> (deg)	90	90	90	90	90
<i>β</i> (deg)	90.355(3)	106.609(10)	90	90.6730(10)	129.4280(10)
<i>γ</i> (deg)	90	90	90	90	90
space group	<i>P2<sub>1</sub>/c</i>	<i>P2<sub>1</sub>/n</i>	<i>Pccn</i>	<i>C2/c</i>	<i>C2/c</i>
<i>Z</i>	4	2	4	4	4
<i>T</i> (K)	100(2)	100(2)	100(2)	100(2)	100(2)
<i>μ</i> (mm <sup>-1</sup> )	0.697	0.988	0.884	1.359	4.723
reflms measd	77969	17453	47979	17887	25718
reflms obsd	13767	17454	6854	4618	7271
<i>R</i> <sub>1</sub> (obsd)	0.0562	0.0766	0.1158	0.0430	0.0915
<i>wR</i> <sub>2</sub> (all data)	0.1435	0.2209	0.2628	0.1164	0.2381

621 potential GANEX process with CyMe<sub>4</sub>-BTBP or CyMe<sub>4</sub>-  
 622 BTPhen. The XAS profiles for the directly synthesized solid  
 623 species (3 and 4) also correlate well with the corresponding  
 624 extracted species (Figures 12 and 13), suggesting that the  
 625 [Ln(CyMe<sub>4</sub>-BTPhen)<sub>2</sub>(H<sub>2</sub>O)]<sup>2+</sup> coordination species found in  
 626 the solid state also exists in the bulk organic-phase  
 627 postextraction.

628 The shells used to fit the EXAFS data for all samples were  
 629 derived from the corresponding Ln<sup>III</sup> structures that have two  
 630 CyMe<sub>4</sub>-BTX (X = BP, Phen) ligands bound to the metal. The

dominant scatter paths include a shell corresponding to the 8 N  
 atoms from the CyMe<sub>4</sub>-BTX ligands that are coordinated to the  
 metal (~2.51 Å) and two shells from the 16 C/N and 16 C  
 atoms located at the ortho and meta positions relative to the  
 coordinating N atoms, respectively (Figure 14). The initial  
 positions of these modeled shells, relative to the central Ln  
 atom, are averaged from the atomic positions obtained from the  
 crystal structures determined by XRD and are located at ~2.51,  
 3.42, and 4.75 Å from the Ln atom for the 8 N, 16 C/N, and 16  
 C shells, respectively (Figure 4 and Tables 8 and 9). It was

Table 6. Selected Interatomic Distances ( $\text{\AA}$ ) for  $\text{CyMe}_4\text{-BTPhen-Containing Complexes 1-5}^a$ 

bond	origin	1 (Pr)	2 (Pr)	3 (Eu)	4 (Tb)	5 (Yb)
N2-M	N <sub>triazinyl</sub>	2.636(9)	2.644(6)	2.539(5)	2.527(5)	2.475(9)
N6-M		2.623(9)	2.635(6)	2.542(5)	2.516(5)	2.507(11)
N10-M		2.623(9)	2.568(6)	N/A	N/A	N/A
N14-M		2.618(8)	2.592(6)	N/A	N/A	N/A
N4-M	N <sub>phen</sub>	2.668(8)	2.632(6)	2.507(5)	2.485(5)	2.422(11)
N5-M		2.644(9)	2.587(6)	2.523(5)	2.499(5)	2.442(10)
N12-M		2.675(8)	2.617(6)	N/A	N/A	N/A
N13-M		2.638(9)	2.583(6)	N/A	N/A	N/A
O1-M	O <sub>water</sub>	N/A	N/A	2.414(6)	2.398(6)	2.373(11)
O1-M	O <sub>nitrate</sub>	2.592(7)	2.581(5)	N/A	N/A	N/A
O2-M		2.544(7)	2.605(5)	N/A	N/A	N/A

<sup>a</sup>N/A = not applicable. The designated bond length does not exist or is symmetry-related to another bond length.

Table 7. Selected Interatomic Distances ( $\text{\AA}$ ) for  $\text{CyMe}_4\text{-BTBP-Containing Complexes 6-10}^a$ 

bond	origin	6 (Pr)	7 (Pr)	8 (Eu)	9 (Eu)	10 (Tb)
N2-M	N <sub>triazinyl</sub>	2.637(5)	2.654(9)	2.565(9)	2.533(4)	2.516(6)
N6-M		2.597(5)	2.595(9)	2.578(10)	N/A	2.512(6)
N10-M		2.611(5)	2.579(9)	N/A	N/A	N/A
N14-M		2.634(6)	2.597(9)	N/A	N/A	N/A
N4-M	N <sub>bipy</sub>	2.638(5)	2.645(9)	2.569(8)	2.545(4)	2.485(5)
N5-M		2.623(5)	2.663(10)	2.562(9)	N/A	2.504(6)
N12-M		2.615(5)	2.650(9)	N/A	N/A	N/A
N13-M		2.633(5)	2.684(9)	N/A	N/A	N/A
O1-M	O <sub>water</sub>	N/A	N/A	N/A	N/A	2.407(8)
O1-M	O <sub>nitrate</sub>	2.596(5)	2.606(8)	2.564(10)	2.548(4)	N/A
O2-M		2.607(5)	2.625(8)	N/A	2.487(3)	N/A
O7-M		N/A	N/A	N/A	2.455(4)	N/A

<sup>a</sup>N/A = not applicable. The designated bond length does not exist or is symmetry-related to another bond length.

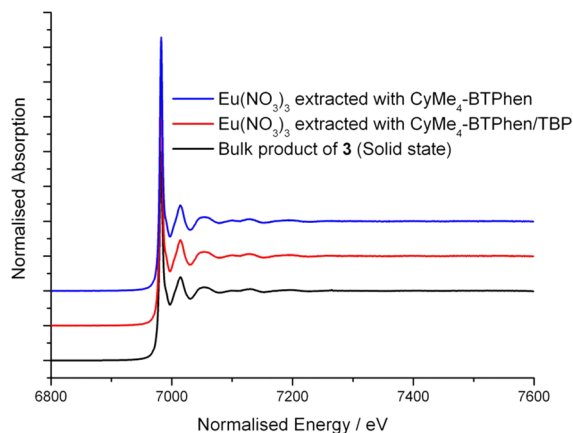


Figure 12. Eu  $L_{\text{III}}$ -edge XAS spectra of  $\text{CyMe}_4\text{-BTPhen-Containing species}$ .

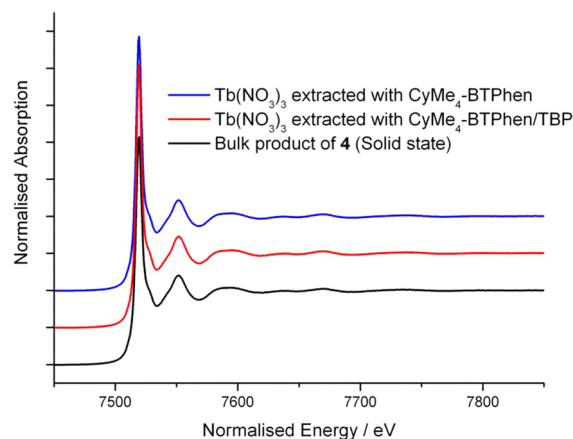


Figure 13. Tb  $L_{\text{III}}$ -edge XAS spectra of  $\text{CyMe}_4\text{-BTPhen-Containing species}$ .

641 found necessary to include an extra shell assigned to 32 C/N  
 642 atoms, initially located at  $\sim 3.40 \text{ \AA}$  from the Ln atom, due to  
 643 multiple scattering from the planar aromatic rings in the N-  
 644 donor ligands in order to obtain appropriate fits (Figure 14). A  
 645 shell corresponding to oxygen coordination at the ninth site  
 646 was included in all fits, initially located at  $2.4\text{--}2.6 \text{ \AA}$  from the  
 647 Ln atom. Two sets of models corresponding to nitrate  
 648 coordination (i.e., O shell occupancy = 2) and water  
 649 coordination (i.e., O shell occupancy = 1) to the lanthanide  
 650 ion were used to fit all EXAFS data in order to ascertain  
 651 whether XAS can be used to distinguish between nitrate and  
 652 water binding in these systems (Tables 8 and 9; see the

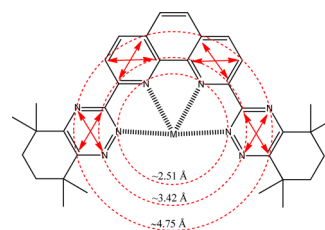


Figure 14. Depiction of the shell occupancy of complexes formed with  $\text{CyMe}_4\text{-BTPhen}$  (or  $\text{CyMe}_4\text{-BTBP}$ ). Also depicted with arrows are some of the multiple scatter paths within the complex.

Table 8. Eu L<sub>III</sub>-Edge EXAFS Data<sup>a</sup>

physical state	aqueous phase	organic-phase extractants	chemical composition used in fitted models	occupancy <sup>b</sup>	interatomic distances from XRD (Å)	fitted interatomic distances <sup>c</sup> (Å)	$\sigma^2$ (Å <sup>2</sup> ) <sup>d</sup>	$r^e$
solution	Eu(NO <sub>3</sub> ) <sub>3</sub>	CyMe <sub>4</sub> -BTBP	[Eu(CyMe <sub>4</sub> -BTBP) <sub>2</sub> (NO <sub>3</sub> ) <sub>2</sub> ] <sup>2+</sup>	Eu–O2	2.56	2.46	0.00200	0.0159
				Eu–N8	2.57	2.59	0.00391	
				Eu–C/ N16	3.44	3.44	0.00731	
				Eu–C/ N32 <sup>f</sup>	3.67	3.68	0.00791	
				Eu–C/ N16	4.78	4.87	0.00374	
solution	Eu(NO <sub>3</sub> ) <sub>3</sub>	CyMe <sub>4</sub> -BTBP + TBP	[Eu(CyMe <sub>4</sub> -BTBP) <sub>2</sub> (NO <sub>3</sub> ) <sub>2</sub> ] <sup>2+</sup>	Eu–O2	2.56	2.55	0.00567	0.0193
				Eu–N8	2.57	2.55	0.00594	
				Eu–C/ N16	3.44	3.45	0.00632	
				Eu–C/ N32 <sup>f</sup>	3.67	3.66	0.00796	
				Eu–C/ N16	4.78	4.87	0.00554	
solution	Eu(NO <sub>3</sub> ) <sub>3</sub>	CyMe <sub>4</sub> -BTPhen	[Eu(CyMe <sub>4</sub> -BTPhen) <sub>2</sub> (NO <sub>3</sub> ) <sub>2</sub> ] <sup>2+</sup>	Eu–O2		2.60	0.00200	0.0206
				Eu–N8	2.51	2.55	0.00493	
				Eu–C/ N16	3.41	3.45	0.00496	
				Eu–C/ N32 <sup>f</sup>	3.65	3.69	0.00800	
				Eu–C/ N16	4.75	4.91	0.00303	
solution	Eu(NO <sub>3</sub> ) <sub>3</sub>	CyMe <sub>4</sub> -BTPhen + TBP	[Eu(CyMe <sub>4</sub> -BTPhen) <sub>2</sub> (NO <sub>3</sub> ) <sub>2</sub> ] <sup>2+</sup>	Eu–O2		2.58	0.00432	0.0222
				Eu–N8	2.51	2.56	0.00486	
				Eu–C/ N16	3.41	3.45	0.00484	
				Eu–C/ N32 <sup>f</sup>	3.65	3.69	0.00800	
				Eu–C/ N16	4.75	4.91	0.00282	
solid	N/A	N/A	[Eu(CyMe <sub>4</sub> -BTPhen) <sub>2</sub> (H <sub>2</sub> O)] <sup>3+</sup>	Eu–O1	2.41	2.57	0.00121	0.0273
				Eu–N8	2.51	2.56	0.00504	
				Eu–C/ N16	3.41	3.44	0.00663	
				Eu–C/ N32 <sup>f</sup>	3.65	3.68	0.00800	
				Eu–C/ N16	4.75	4.92	0.00944	
			[Eu(CyMe <sub>4</sub> -BTPhen) <sub>2</sub> (NO <sub>3</sub> ) <sub>2</sub> ] <sup>2+</sup>	Eu–O2		2.56	0.00193	0.0231
				Eu–N8	2.51	2.56	0.00667	
				Eu–C/ N16	3.41	3.43	0.00605	
				Eu–C/ N32 <sup>f</sup>	3.65	3.68	0.00800	
				Eu–C/ N16	4.75	4.91	0.00763	

<sup>a</sup>S<sub>0</sub><sup>2</sup> is fitted but constrained to be within the range of 0.8–1.0 and the same value for all shells. <sup>b</sup>Occupancy numbers, held constant at given values. <sup>c</sup>±0.02 Å. <sup>d</sup>Debye–Waller factors. <sup>e</sup>Parameter describing goodness of fit = weighted sum of squares of residuals divided by the degree of freedom. <sup>f</sup>Shell due to multiple scattering.

Supporting Information). The EXAFS data fits were obtained by allowing the shell distances to be refined, while the shell occupancies were fixed at chosen integer values. Attempts were made to fit the EXAFS data to a model corresponding to the coordination of one molecule of CyMe<sub>4</sub>-BTX with three nitrate molecules occupying the remaining coordination sites, but these did not give any statistically justifiable fits.

Fits for all of the EXAFS data obtained, using a model relating to the coordination of two CyMe<sub>4</sub>-BTX molecules gave very good statistical correlations (Figure 15 and Tables 8 and 9; see the Supporting Information), indicating that the predominant lanthanide species in the bulk organic phase formed by extraction with these tetra-N-donor molecules is a 1:2 Ln<sup>3+</sup>/CyMe<sub>4</sub>-BTX complex. The refined radial distances for the three closest N-donor ligand-based shells to the Ln center

Table 9. Tb L<sub>III</sub>-Edge EXAFS Data<sup>a</sup>

physical state	aqueous phase	organic-phase extractants	chemical composition used in fitted models	occupancy <sup>b</sup>	interatomic distances from XRD (Å)	fitted interatomic distances (Å) <sup>c</sup>	$\sigma^2$ (Å <sup>2</sup> ) <sup>d</sup>	$r^e$
solution	Tb(NO <sub>3</sub> ) <sub>3</sub>	CyMe <sub>4</sub> -BTBP	[Tb(CyMe <sub>4</sub> -BTBP) <sub>2</sub> (NO <sub>3</sub> ) <sub>2</sub> ] <sup>2+</sup>	Tb–O2		2.53	0.00347	0.0140
				Tb–N8	2.50	2.51	0.00654	
				Tb–C/ N16	3.38	3.39	0.00530	
				Tb–C/ N32 <sup>f</sup>	3.61	3.65	0.00800	
				Tb–C/ N16	4.72	4.83	0.00165	
solution	Tb(NO <sub>3</sub> ) <sub>3</sub>	CyMe <sub>4</sub> -BTBP + TBP	[Tb(CyMe <sub>4</sub> -BTBP) <sub>2</sub> (NO <sub>3</sub> ) <sub>2</sub> ] <sup>2+</sup>	Tb–O2		2.52	0.00365	0.0146
				Tb–N8	2.50	2.51	0.00675	
				Tb–C/ N16	3.38	3.40	0.00576	
				Tb–C/ N32 <sup>f</sup>	3.61	3.64	0.00800	
				Tb–C/ N16	4.72	4.83	0.00160	
solution	Tb(NO <sub>3</sub> ) <sub>3</sub>	CyMe <sub>4</sub> -BTPhen	[Tb(CyMe <sub>4</sub> -BTPhen) <sub>2</sub> (NO <sub>3</sub> ) <sub>2</sub> ] <sup>2+</sup>	Tb–O2		2.52	0.00210	0.0133
				Tb–N8	2.52	2.52	0.00840	
				Tb–C/ N16	3.40	3.40	0.00570	
				Tb–C/ N32 <sup>f</sup>	3.62	3.66	0.00800	
				Tb–C/ N16	4.73	4.84	0.00190	
solution	Tb(NO <sub>3</sub> ) <sub>3</sub>	CyMe <sub>4</sub> -BTPhen + TBP	[Tb(CyMe <sub>4</sub> -BTPhen) <sub>2</sub> (NO <sub>3</sub> ) <sub>2</sub> ] <sup>2+</sup>	Tb–O2		2.53	0.00204	0.0134
				Tb–N8	2.52	2.51	0.00835	
				Tb–C/ N16	3.40	3.40	0.00537	
				Tb–C/ N32 <sup>f</sup>	3.62	3.66	0.00800	
				Tb–C/ N16	4.73	4.84	0.00185	
solid	N/A	N/A	[Tb(CyMe <sub>4</sub> -BTPhen) <sub>2</sub> (H <sub>2</sub> O)] <sup>3+</sup>	Tb–O1	2.40	2.54	0.00196	0.0166
				Tb–N8	2.52	2.52	0.00620	
				Tb–C/ N16	3.40	3.41	0.00601	
				Tb–C/ N32 <sup>f</sup>	3.62	3.66	0.00800	
				Tb–C/ N16	4.73	4.85	0.00532	
		N/A	[Tb(CyMe <sub>4</sub> -BTPhen) <sub>2</sub> (NO <sub>3</sub> ) <sub>2</sub> ] <sup>2+</sup>	Tb–O2		2.53	0.00199	0.0141
				Tb–N8	2.52	2.52	0.00772	
				Tb–C/ N16	3.40	3.40	0.00529	
				Tb–C/ N32 <sup>f</sup>	3.62	3.66	0.00800	
				Tb–C/ N16	4.73	4.84	0.00324	

<sup>a</sup>S<sub>0</sub><sup>2</sup> is fitted but constrained to be within the range of 0.8–1.0 and the same value for all shells. <sup>b</sup>Occupancy numbers, held constant at given values. <sup>c</sup>±0.02 Å. <sup>d</sup>Debye–Waller factors. <sup>e</sup>Parameter describing goodness of fit = weighted sum of squares of residuals divided by the degree of freedom. <sup>f</sup>Shell due to multiple scattering.

668 (i.e., 8 N, 16 C/N, and 32 C/N shells) generally only show  
669 minimal shifts from the initial input values derived from the  
670 structural information obtained by XRD (Tables 8 and 9; see  
671 the Supporting Information). The radial distance of the 16 C  
672 shell does typically refine to a slightly larger value (4.80–4.95  
673 Å) relative to the initial input value (4.70–4.80 Å) for the  
674 extracted solutions and solid-state samples. This suggests that  
675 either this outer C shell is influenced by multiple scattering

676 effects or some fluctuation of the N<sub>4</sub>-donor ligand occurs at the  
677 outer regions of these lanthanide complexes. No significant  
678 differences in the refined radial distances are observed in the  
679 extracted samples when TBP is present or not, providing  
680 further proof that TBP that does not influence Ln<sup>3+</sup> speciation  
681 in a GANEX process with CyMe<sub>4</sub>-BTX and TBP in the organic  
682 phase.

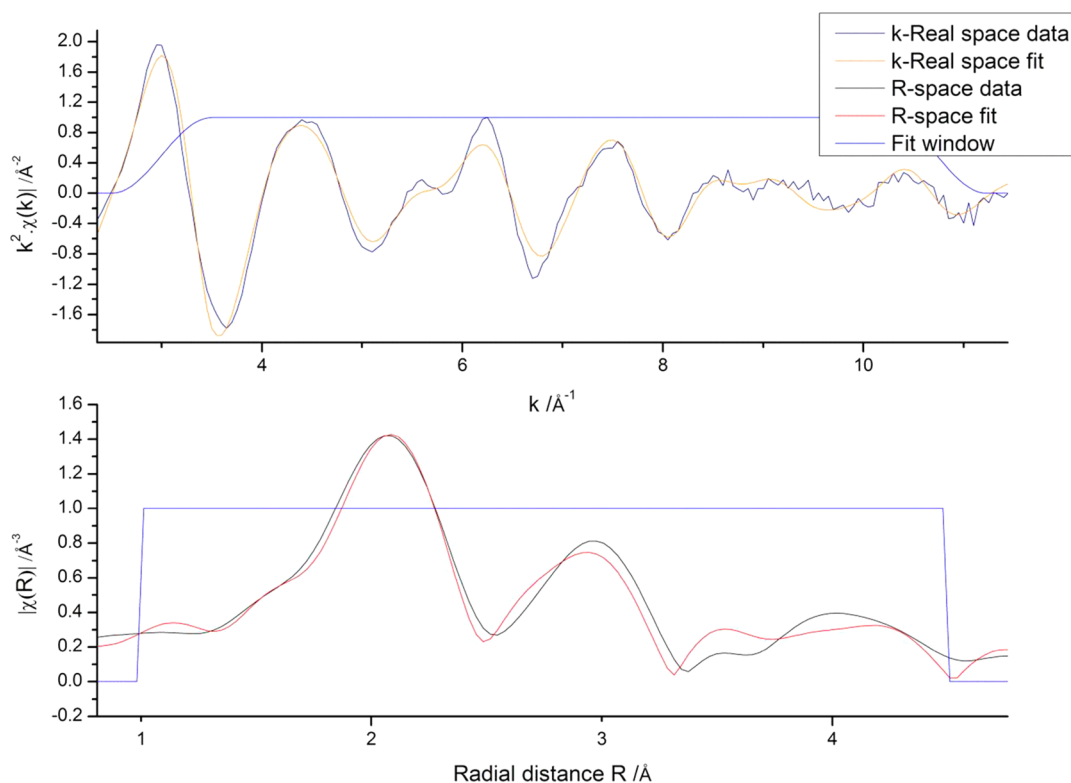


**Figure 15.** Eu L<sub>III</sub>-edge EXAFS spectrum in  $k$  space (upper plot) and its Fourier transform in  $R$  space (lower plot) of the extraction of  $\text{Eu}(\text{NO}_3)_3$  (10 mM) from an aqueous solution (1 M  $\text{HNO}_3$  and 3 M  $\text{NaNO}_3$ ) into cyclohexanone with  $\text{CyMe}_4\text{-BTPPh}$  (50 mM). The data are fitted to the model complex  $[\text{Eu}(\text{CyMe}_4\text{-BTPPh})_2(\text{NO}_3)_2]^{2+}$ .

683 The identity of the ninth coordination site species cannot be  
 684 unambiguously assigned from the EXAFS data because the fits  
 685 are unable to resolve the relatively small change between nitrate  
 686 and water coordination at this site. Both sets of models, either  
 687 with water or nitrate bound at the ninth coordination site,  
 688 provided fits with very good statistical correlations (Tables 8  
 689 and 9; see the Supporting Information). The fits for all of the  
 690 Eu L<sub>III</sub>-edge data (Table 8; see the Supporting Information)  
 691 show that the first O shell refines to give Eu–O distances  
 692 between 2.46 and 2.60 Å. There is little distinction between the  
 693 refined Eu–O distances when the shell occupancy is fixed at 1  
 694 (for water coordination) or 2 (for nitrate coordination). The  
 695 refined Eu–O<sub>nitrate</sub> distances agree with those bond lengths  
 696 determined for structures 8 [2.56(1) Å] and 9 [2.548(4) Å]  
 697 and fall within the range of all known Eu–O<sub>nitrate</sub> distances  
 698 (2.31–2.82 Å) established by crystallography.<sup>35,38</sup> The refined  
 699 Eu–O<sub>water</sub> distances also fall within the wide range of Eu–O<sub>water</sub>  
 700 bond lengths from previously reported structures (2.27–2.72  
 701 Å)<sup>35,39</sup> but are larger than this distance in complex 3 [2.414(6)  
 702 Å]. The O shells for all of the Tb L<sub>III</sub>-edge EXAFS spectra  
 703 modeled with either water or nitrate coordination (Table 9; see  
 704 the Supporting Information) all refine to within a narrow range  
 705 of 2.52–2.54 Å from the Tb center and fall within the relatively  
 706 wide range of known Tb–O<sub>nitrate</sub> (2.19–2.85 Å)<sup>35,40</sup> and Tb–  
 707 O<sub>water</sub> bond lengths (2.27–2.70 Å).<sup>35,39</sup> As is similarly observed  
 708 in the equivalent europium studies, all of the Tb–O<sub>water</sub>  
 709 distances refined from the EXAFS data are larger than that  
 710 observed in complex 4 [2.397(6) Å] by XRD. The refined  
 711 radial distances for these low-occupancy O shells generally  
 712 match the refined location for the dominant 8 N shell from the  
 713 coordinating N-donor ligands even when these distances are  
 714 expected to be different. This is particularly evident in the

EXAFS fits of complexes 3 and 4 in the solid state, which have  
 also been characterized by XRD. The refined distances for the  
 O shells obtained from the fits of the EXAFS data in these  
 solid-state samples (Eu–O for 3 = 2.57 Å; Tb–O for 4 = 2.54  
 Å) are distinctly longer than those observed by XRD [Eu–O  
 for 3 = 2.414(6) Å; Tb–O for 4 = 2.397(6) Å] and are similar  
 to the refined radial distances of the 8 N shell (Eu–N for 3 =  
 2.56 Å; Tb–N for 4 = 2.52 Å). It may be that the high-  
 occupancy 8 N shell is masking the contribution of the lower-  
 occupancy (1 or 2) O shell.

## EXPERIMENTAL SECTION

**General Procedures.** Elemental analyses were performed with a  
 Carlo Erba Instruments CHNS-O EA1108 elemental analyzer for  
 carbon, hydrogen, and nitrogen and a Fisons Horizon elemental  
 analysis ICP-OES spectrometer for praseodymium, europium, and  
 terbium. ESI-MS (positive ion) was performed using a Micromass  
 Platform spectrometer. Solution UV–visible spectra were recorded on  
 a PG Instruments T60U spectrophotometer with a fixed spectral  
 bandwidth of 2 nm. Typical scan ranges were 200–500 nm at a scan  
 rate of ~390 nm min<sup>-1</sup>. Excitation and emission spectra were recorded  
 with Edinburgh Instrument FP920 phosphorescence lifetime spec-  
 trometer equipped with a 5 W microsecond-pulsed xenon flashlamp  
 (with single 300 mm focal length excitation and emission  
 monochromators in a Czerny Turner configuration) and a red-  
 sensitive photomultiplier in Peltier (air-cooled) housing (Hamamatsu  
 R928P) using a gate time of 0.05 ms and a delay time of 0.5 ms.  
 Excitation spectra were obtained using the following emission  
 wavelengths: Eu<sup>3+</sup>, 616 nm; Tb<sup>3+</sup>, 545 nm. Lifetime data were  
 recorded following 320 nm excitation with a microsecond-pulsed  
 xenon flashlamp (Edinburgh Instruments) using the multichannel  
 scaling method. Lifetimes were obtained by a tail fit on the data  
 obtained, and the quality of the fit was judged by minimization of  
 reduced  $\chi^2$  and residuals squared. Where the decay profiles are

748 reported as monoexponential, fitting to a double-exponential decay  
749 yielded no improvement in the fit, as judged by minimization of  
750 residuals squared and reduced  $\chi^2$ .

751 **Syntheses and Solution Preparations.** All chemicals were  
752 purchased from Sigma Aldrich and were used as supplied. CyMe<sub>4</sub>-  
753 BTPPhen and CyMe<sub>4</sub>-BTBP were synthesized as previously de-  
754 scribed<sup>20,23</sup> but using an improved purification methodology.

755 **Purification of CyMe<sub>4</sub>-BTPPhen and CyMe<sub>4</sub>-BTBP.** The crude  
756 product of CyMe<sub>4</sub>-BTPPhen or CyMe<sub>4</sub>-BTBP was dissolved in DCM  
757 and loaded onto a column of silica resin. The column was washed with  
758 neat DCM, quickly eluting a yellow solution and leaving a dark-  
759 orange/brown band at the top of the column. The solvent was  
760 removed from the yellow eluent by rotary evaporation, yielding a  
761 vibrant-yellow powder, which was found to be pure by NMR  
762 spectroscopy. The purified product was found to be soluble in DCM,  
763 cyclohexanone, and 1-octanol up to concentrations of 5 mM. Further  
764 purified CyMe<sub>4</sub>-BTPPhen/CyMe<sub>4</sub>-BTBP could be obtained by elution  
765 with 1–5% (v/v) MeOH in DCM from the silica column.

766 **Synthesis of Pr<sup>3+</sup> Complexes with CyMe<sub>4</sub>-BTPPhen.** A solution  
767 of Pr(NO<sub>3</sub>)<sub>3</sub>·6H<sub>2</sub>O (23 mg, 54 μmol) in CH<sub>3</sub>CN (5 mL) was added  
768 to a solution of CyMe<sub>4</sub>-BTPPhen (30 mg, 54 μmol) in DCM (5 mL)  
769 and left standing to evaporate to dryness. The resultant powder was  
770 dissolved in a mixture of CH<sub>3</sub>CN (2 mL), DCM (2 mL), and EtOH  
771 (0.5 mL) and again allowed to evaporate slowly in order to crystallize.  
772 A yellow platelike crystal was selected from the isolated material, and  
773 XRD analysis indicated that the composition of the crystal was of the  
774 formulation [Pr(CyMe<sub>4</sub>-BTPPhen)<sub>2</sub>(NO<sub>3</sub>)<sub>2</sub>](NO<sub>3</sub>)<sub>2</sub>·10H<sub>2</sub>O (1·10H<sub>2</sub>O).  
775 Elemental analysis of the isolated material indicated that the  
776 composition of the bulk product was of the formulation [Pr(CyMe<sub>4</sub>-  
777 BTPPhen)<sub>2</sub>(NO<sub>3</sub>)<sub>2</sub>][Pr(NO<sub>3</sub>)<sub>3</sub>·2H<sub>2</sub>O (2·2H<sub>2</sub>O)]. Elem anal. Calcd for  
778 [(C<sub>34</sub>H<sub>38</sub>N<sub>8</sub>)<sub>2</sub>(NO<sub>3</sub>)<sub>2</sub>Pr][Pr(NO<sub>3</sub>)<sub>3</sub>·2H<sub>2</sub>O]: C, 45.19; H, 4.46; N,  
779 17.05; Pr, 15.59. Found: C, 45.01; H, 4.08; N, 16.90; Pr, 15.23. The  
780 bulk material was dissolved in EtOH (1 mL) and allowed to slowly  
781 evaporate over 1 week, yielding yellow blocklike crystals suitable for  
782 single-crystal XRD analysis (yield = 0.03 g). ESI-MS (positive ion): *m/z*  
783 *z* 659 ([C<sub>34</sub>H<sub>38</sub>N<sub>8</sub>)<sub>2</sub>(NO<sub>3</sub>)<sub>2</sub>Pr]<sup>2+</sup>). UV–visible spectrum (MeOH)  
784 [ $\lambda_{\text{max}}/\text{nm}$  ( $\epsilon_{\text{max}}/\text{L mol}^{-1} \text{cm}^{-1}$ ): 266 (71000), 321 (38000)].

785 **Synthesis of [Eu(CyMe<sub>4</sub>-BTPPhen)<sub>2</sub>(H<sub>2</sub>O)](NO<sub>3</sub>)<sub>3</sub>·2H<sub>2</sub>O  
786 (3·2H<sub>2</sub>O).** A solution of Eu(NO<sub>3</sub>)<sub>3</sub>·6H<sub>2</sub>O (24 mg, 54 μmol) in  
787 CH<sub>3</sub>CN (5 mL) was added to a solution of CyMe<sub>4</sub>-BTPPhen (30 mg,  
788 54 μmol) in DCM (5 mL) and left standing to evaporate to dryness.  
789 The resultant powder was dissolved in a mixture of CH<sub>3</sub>CN (2 mL),  
790 DCM (2 mL), and EtOH (0.5 mL) and allowed to evaporate slowly,  
791 yielding yellow blocklike crystals suitable for single-crystal XRD  
792 analysis (yield = 0.02 g). Elem anal. Calcd for [(C<sub>34</sub>H<sub>38</sub>N<sub>8</sub>)<sub>2</sub>(H<sub>2</sub>O)-  
793 Eu](NO<sub>3</sub>)<sub>3</sub>·2H<sub>2</sub>O: C, 54.11; H, 5.48; N, 17.63; Eu, 10.07. Found: C,  
794 54.18; H, 5.07; N, 17.61; Eu, 10.51. ESI-MS (positive ion): *m/z* 666  
795 ([C<sub>34</sub>H<sub>38</sub>N<sub>8</sub>)<sub>2</sub>(NO<sub>3</sub>)<sub>2</sub>Eu]<sup>2+</sup>). UV–visible spectrum (MeOH) [ $\lambda_{\text{max}}/\text{nm}$   
796 ( $\epsilon_{\text{max}}/\text{L mol}^{-1} \text{cm}^{-1}$ ): 266 (99000), 321 (52000)].

797 **Synthesis of [Tb(CyMe<sub>4</sub>-BTPPhen)<sub>2</sub>(H<sub>2</sub>O)](NO<sub>3</sub>)<sub>3</sub>·H<sub>2</sub>O (4·H<sub>2</sub>O).**  
798 The synthesis was performed as described for 2 except using  
799 Tb(NO<sub>3</sub>)<sub>3</sub>·5H<sub>2</sub>O (17 mg, 38 μmol) and CyMe<sub>4</sub>-BTPPhen (21 mg,  
800 38 μmol) as the initial reagents. Yellow platelike crystals suitable for  
801 single-crystal XRD analysis were obtained (yield = 0.02 g). Elem anal.  
802 Calcd for [(C<sub>34</sub>H<sub>38</sub>N<sub>8</sub>)<sub>2</sub>(H<sub>2</sub>O)Tb](NO<sub>3</sub>)<sub>3</sub>·H<sub>2</sub>O: C, 54.51; H, 5.38; N,  
803 17.76; Tb, 10.61. Found: C, 54.69; H, 5.17; N, 17.73; Tb, 9.82. ESI-  
804 MS (positive ion): *m/z* 669 ([C<sub>34</sub>H<sub>38</sub>N<sub>8</sub>)<sub>2</sub>(NO<sub>3</sub>)<sub>2</sub>Tb]<sup>2+</sup>). UV–visible  
805 spectrum (MeOH) [ $\lambda_{\text{max}}/\text{nm}$  ( $\epsilon_{\text{max}}/\text{L mol}^{-1} \text{cm}^{-1}$ ): 265 (96000), 322  
806 (51000)].

807 **Synthesis of [Yb(CyMe<sub>4</sub>-BTPPhen)<sub>2</sub>(H<sub>2</sub>O)](NO<sub>3</sub>)<sub>3</sub>·3H<sub>2</sub>O  
808 (5·3H<sub>2</sub>O).** The synthesis was performed as described for 2 except  
809 using Yb(NO<sub>3</sub>)<sub>3</sub>·5H<sub>2</sub>O (24 mg, 54 μmol) and CyMe<sub>4</sub>-BTPPhen (30  
810 mg, 54 μmol) as the initial reagents. Yellow rhombohedron-like  
811 crystals suitable for single-crystal XRD analysis were obtained (yield <  
812 0.01 g). ESI-MS (positive ion): *m/z* 677 ([C<sub>34</sub>H<sub>38</sub>N<sub>8</sub>)<sub>2</sub>(NO<sub>3</sub>)<sub>2</sub>Yb]<sup>2+</sup>).  
813

814 **Synthesis of Ln<sup>3+</sup> Complexes with CyMe<sub>4</sub>-BTBP.** A solution of  
815 CyMe<sub>4</sub>-BTBP (30 mg, 56 μmol) in DCM (1 mL) was added to a  
816 solution of Ln(NO<sub>3</sub>)<sub>3</sub>·xH<sub>2</sub>O [Pr(NO<sub>3</sub>)<sub>3</sub>·6H<sub>2</sub>O, 12 mg, 28 μmol;  
817 Eu(NO<sub>3</sub>)<sub>3</sub>·6H<sub>2</sub>O, 13 mg, 28 μmol; Tb(NO<sub>3</sub>)<sub>3</sub>·5H<sub>2</sub>O, 12 mg, 28 μmol]  
818 in MeOH (1 mL). CH<sub>3</sub>CN (1.5 mL) was added to the reaction

819 mixture, and the solution was allowed to evaporate to dryness. Once  
820 dry, toluene (1.25 mL), EtOH (1.25 mL), <sup>i</sup>PrOH (1.25 mL), and  
821 DCM (1.25 mL) were added to dissolve the residues, and the  
822 solutions were allowed to evaporate slowly. Crystals suitable for single-  
823 crystal XRD were obtained over several weeks. The mixtures afforded a  
824 variety of crystals of varying compositions determined by single-crystal  
825 XRD analysis to be [Pr(CyMe<sub>4</sub>-BTBP)<sub>2</sub>(NO<sub>3</sub>)<sub>2</sub>](NO<sub>3</sub>)<sub>2</sub>·4EtOH·H<sub>2</sub>O  
826 (6·4EtOH·H<sub>2</sub>O), [Pr(CyMe<sub>4</sub>-BTBP)<sub>2</sub>(NO<sub>3</sub>)<sub>2</sub>][Pr(NO<sub>3</sub>)<sub>3</sub>·6H<sub>2</sub>O]  
827 (NO<sub>3</sub>)<sub>2</sub>·6CH<sub>3</sub>CN (7·6CH<sub>3</sub>CN), [Eu(CyMe<sub>4</sub>-BTBP)<sub>2</sub>(NO<sub>3</sub>)<sub>2</sub>]-  
828 (NO<sub>3</sub>)<sub>2</sub>·4EtOH·2H<sub>2</sub>O (8·4EtOH·2H<sub>2</sub>O), [Eu(CyMe<sub>4</sub>-BTBP)-  
829 (NO<sub>3</sub>)<sub>3</sub>]<sub>2</sub>·toluene (9·toluene), and [Tb(CyMe<sub>4</sub>-BTBP)<sub>2</sub>(H<sub>2</sub>O)]-  
830 (NO<sub>3</sub>)<sub>2</sub>·4EtOH (10·4EtOH). Bulk analysis of the crystallized  
831 samples by ESI-MS provided the following data:-

832 ESI-MS (positive ion): Pr<sup>3+</sup> complexation, *m/z* 635  
833 ([C<sub>32</sub>H<sub>38</sub>N<sub>8</sub>)<sub>2</sub>(NO<sub>3</sub>)<sub>2</sub>Pr]<sup>2+</sup>); Eu<sup>3+</sup> complexation, *m/z* 641  
834 ([C<sub>32</sub>H<sub>38</sub>N<sub>8</sub>)<sub>2</sub>(NO<sub>3</sub>)<sub>2</sub>Eu]<sup>2+</sup>); Tb<sup>3+</sup> complexation, *m/z* 643  
835 ([C<sub>32</sub>H<sub>38</sub>N<sub>8</sub>)<sub>2</sub>(NO<sub>3</sub>)<sub>2</sub>Tb]<sup>2+</sup>).  
836

837 **Solution Preparation for UV–visible Spectroscopic Studies  
838 of Ln<sup>3+</sup> Complexation with CyMe<sub>4</sub>-BTPPhen and CyMe<sub>4</sub>-BTBP.**  
839 Methanolic solutions of the ligands CyMe<sub>4</sub>-BTBP and CyMe<sub>4</sub>-BTPPhen  
840 (1.0 × 10<sup>-4</sup> M, 0.4 mL) were added to a quartz cuvette of 1 cm path  
841 length, and the solutions were diluted to 2 mL with MeOH (2.0 ×  
842 10<sup>-5</sup> M). At this point, an initial spectrum of the ligand was recorded.  
843 Metal solutions of Eu(NO<sub>3</sub>)<sub>3</sub>·6H<sub>2</sub>O, Pr(NO<sub>3</sub>)<sub>3</sub>·6H<sub>2</sub>O, and Tb-  
844 (NO<sub>3</sub>)<sub>3</sub>·5H<sub>2</sub>O (4.0 × 10<sup>-4</sup> M) in MeOH were used. For each  
845 titration, the metal solution was added into the cuvette in 10 μL (4.0 ×  
846 10<sup>-9</sup> mol, 0.10 equiv) aliquots and shaken, and spectra were recorded  
847 after each addition up to a ratio of 1.5:1 metal/ligand. At this point,  
848 the aliquot size was increased to 50 μL (0.50 equiv) to a final ratio of  
849 3:1 metal/ligand.  
850

851 **Solution Preparation for Luminescence Studies of Ln<sup>3+</sup> (Ln  
852 = Pr, Tb, Eu) Complexation with CyMe<sub>4</sub>-BTPPhen and CyMe<sub>4</sub>-  
853 BTBP.** A solution of CyMe<sub>4</sub>-BTPPhen/CyMe<sub>4</sub>-BTBP in MeOH (120  
854 μL, 1 × 10<sup>-4</sup> M) was added to a 1.2 mL quartz cuvette followed by the  
855 addition of a solution of Ln(NO<sub>3</sub>)<sub>3</sub> in MeOH (20 μL, 3 × 10<sup>-4</sup> M).  
856 The solution was diluted to ~1 mL with MeOH, and spectra were  
857 obtained.  
858

859 Solution samples in MeOH-*d*<sub>4</sub> were prepared in the same manner as  
860 that for the MeOH samples but using a 6 × 10<sup>-4</sup> M solution of  
861 CyMe<sub>4</sub>-BTPPhen/CyMe<sub>4</sub>-BTBP (20 μL) in MeOH-*d*<sub>4</sub>, and solutions  
862 were diluted using MeOH-*d*<sub>4</sub>.  
863

864 **Extracted Sample Preparation for XAS Measurements.**  
865 Predistilled cyclohexanone and a 30% (v/v) solution of TBP in  
866 cyclohexanone were “washed” before use according to previously  
867 outlined procedures.<sup>41</sup> The washing of the organic solvent took place  
868 days before lanthanide extractions were performed. The extractants  
869 CyMe<sub>4</sub>-BTBP and CyMe<sub>4</sub>-BTPPhen were dissolved in either solvent  
870 system by gentle warming and sonication to a final extractant  
871 concentration of 50 mM. Aqueous stock solutions of Ln(NO<sub>3</sub>)<sub>3</sub> (Ln =  
872 Pr, Eu, Tb; 10 mM) were prepared by dissolution of the relevant salt  
873 in 4 M HNO<sub>3</sub> in deionized H<sub>2</sub>O for extractions with 30% TBP/  
874 cyclohexanone, while an aqueous mixture of 1 M HNO<sub>3</sub> and 3 M  
875 NaNO<sub>3</sub> in deionized water was used for extractions with pure  
876 cyclohexanone because of previously reported miscibility issues.<sup>22</sup>  
877

878 The extractions were performed using 1.0 mL of each phase  
879 (organic and aqueous) contained in a 2.5 mL sample vial. The phases  
880 were mixed using a Labinco L46 shaker for 5 min each. Once  
881 contacted, each sample had the (lower) aqueous layer syringed out of  
882 the vial and then the (upper) organic layer pipetted into another vial  
883 for storage before XAS measurements were performed.  
884

885 **Solid Sample Preparation for XAS Measurements.** Solid  
886 samples of 2–4 were prepared for XAS measurements by crushing  
887 ~5–6 mg of the crystalline material in a mortar and pestle and mixed  
888 thoroughly with ~90 mg of BN. The homogeneous material was then  
889 pressed into flat disks (~2 cm diameter).  
890

891 **X-ray Crystallography.** Diffraction data for 1·10H<sub>2</sub>O,  
892 2·1.63EtOH·0.75H<sub>2</sub>O, 3·9H<sub>2</sub>O, 4·9H<sub>2</sub>O, 5·9H<sub>2</sub>O, 6·4EtOH·H<sub>2</sub>O,  
893 7·6CH<sub>3</sub>CN, 8·4EtOH·2H<sub>2</sub>O, 9·toluene, and 10·4EtOH were meas-  
894 ured at 100 K with either a Bruker APEX SMART platform CCD area  
895 Mo K $\alpha$  diffractometer (2, 3, and 9), an Oxford Diffraction XCalibur2  
896

888 Mo  $K\alpha$  diffractometer (1 and 4–8), or a Bruker APEX2 Cu  $K\alpha$   
889 diffractometer (10). All were equipped with a low-temperature device,  
890 and collections were performed at 100 K. *CryAlisPro* was used to guide  
891 the Oxford diffractometer for collection of a full set of diffraction  
892 images and perform unit cell determination and data reduction. These  
893 data were corrected for Lorenz and polarization factors, and analytical,  
894 multiscan, and absorption corrections were applied. Bruker SMART  
895 (Mo  $K\alpha$ ) or APEX2 (Cu  $K\alpha$ ) was used to guide the Bruker  
896 diffractometers and perform unit cell determinations.<sup>42</sup> Reduction of  
897 the Bruker collected data was performed using *SAINTE PLUS* (Mo  $K\alpha$ )  
898 or APEX2 (Cu  $K\alpha$ ), and a multiscan absorption correction was  
899 performed using *SADABS*.<sup>43,44</sup> For all crystal data, the structures were  
900 solved by direct methods using *SIR92*.<sup>45</sup> Structure refinement was  
901 achieved via full-matrix least squares based on  $F^2$  using *SHELXL97*.<sup>46</sup>  
902 All non-H atoms not exhibiting disorder were refined anisotropically,  
903 while H atoms were included in calculated positions. Molecular  
904 graphics were generated using *ORTEP*, and all displayed plots show  
905 probability ellipsoids of 50%.<sup>47</sup> In the case of structure 10, modeling of  
906 residual solvent molecules was not possible. As such, the *SQUEEZE*  
907 procedure in *PLATON* was used to obtain solvent-free reflection data,  
908 and subsequent refinement was performed on these data. The *PART*  
909 command was used to model disorder over multiple sites, where  
910 appropriate, and is detailed in the relevant CIF (crystallographic  
911 information) files (see the Supporting Information).

912 **General XAS Measurements.** Ln (Eu and Tb)  $L_{III}$ -edge XAS  
913 spectra of extracted solutions and crystalline solids were recorded in  
914 transmission and fluorescence modes on Beamline B18 at the  
915 Diamond Light Source operating in a 10 min top-up mode for a  
916 ring current of 300 mA and an energy of 3 GeV. The radiation was  
917 monochromated with a Si(111) double crystal, and harmonic rejection  
918 was achieved through the use of two platinum-coated mirrors  
919 operating at an incidence angle of 8.3 mrad. The monochromator  
920 was calibrated using the K-edge of an iron foil, taking the first  
921 inflection point in the Fe-edge as 7112 eV. Spectra obtained in  
922 fluorescence mode utilized a nine-element germanium detector. The  
923 spectra were summed and background-subtracted using the software  
924 package *Athena*.<sup>48</sup> The spectra were simulated using the software  
925 package *Artemis*, which utilizes the Feff database in its simulations.<sup>48,49</sup>

## 926 ■ CONCLUSIONS

927 The successful characterization of a series of directly  
928 synthesized Ln<sup>III</sup> complexes of the tetra-N-donor extractants  
929 CyMe<sub>4</sub>-BTPhen and CyMe<sub>4</sub>-BTBP using XRD for solid-state  
930 studies and solution electronic spectroscopy has provided  
931 robust chemical models, which can be used to assist in the  
932 determination of lanthanide species formed under proposed  
933 conditions for the partitioning of SNF. Fits of the EXAFS  
934 region from XAS spectra showed that the dominant species  
935 extracted into the organic phase were complex, where two N<sub>4</sub>-  
936 donor extractant ligands were coordinated to the Ln<sup>3+</sup> center, as  
937 is mainly observed in the direct synthesis studies. XAS was  
938 unable to elucidate the bound ligand at the ninth coordination  
939 site in these Ln<sup>3+</sup> complexes, but luminescence spectroscopy  
940 indicates that nitrate coordination is preferred over water  
941 binding in organic solvents. The presence of TBP in the organic  
942 phase, which may be used in a potential GANEX separation,  
943 clearly showed no influence with regards to lanthanide  
944 speciation. Further work will assess the source of the high  
945 separation factors that these N-donor ligands exhibit for minor  
946 actinide/lanthanide partitioning. Similar speciation studies for  
947 extracted Am<sup>3+</sup> and Cm<sup>3+</sup> in the bulk organic phase will be  
948 performed to determine if minor actinide complexes analogous  
949 to those observed in the lanthanide studies are formed or  
950 whether separation is achieved by the formation of minor  
951 actinide species that are substantially different [e.g., charge-  
952 neutral tris(nitrate) complex molecules] from those of the

lanthanides. Such studies have been performed for BTP-derived  
extractants and indicate little difference between Eu<sup>3+</sup> and Cm<sup>3+</sup>  
speciation,<sup>50</sup> but this needs to be confirmed for the N<sub>4</sub>-donor  
extractants particularly with respect to the role of nitrate ions as  
the lanthanide series is traversed in minor actinide/lanthanide  
coordination. Studies investigating metal speciation at the  
interfacial region in these liquid–liquid separations will also be  
conducted to assess the mechanism by which the minor  
actinides preferentially cross from the aqueous phase into the  
organic phase using these organic-soluble N-donor extractants  
and whether actinide/lanthanide speciation in the bulk organic  
phase is different from that at the liquid–liquid interface.  
Understanding the molecular-scale processes that underpin  
techniques for the partitioning of SNF will provide improved  
development of advanced separation methodologies like  
SANEX and GANEX.

## ■ ASSOCIATED CONTENT

### Supporting Information

Plots of single-crystal XRD structures, crystallographic  
information files (CIF), UV–visible absorption, excitation  
and emission spectra, ORTEP plots, and XAS spectra with  
corresponding fits and parameters for the EXAFS data region.  
This material is available free of charge via the Internet at  
<http://pubs.acs.org>.

## ■ AUTHOR INFORMATION

### Corresponding Author

\*E-mail: [clint.a.sharrad@manchester.ac.uk](mailto:clint.a.sharrad@manchester.ac.uk). Tel: +44 161 275  
4657. Fax: +44 161 306 9321.

### Notes

The authors declare no competing financial interest.

## ■ ACKNOWLEDGMENTS

This work is funded by the RCUK Energy Programme through  
its support of the MBASE consortium and the Nuclear Fission  
Safety Program of the European Union through ACSEPT  
Contract FP7-CP-2007-211 267. The studentship for D.M.W.  
was provided by the EPSRC-funded Nuclear FiRST Doctoral  
Training Centre. We thank Diamond Light Source for access to  
Beamline B18 (SP7226), which contributed to the results  
presented here. We acknowledge use of the EPSRC-funded  
Chemical Database Service at Daresbury. We also thank Dr.  
John Charnock for his assistance with EXAFS simulations. Use  
of the Chemical Analysis Facility at the University of Reading  
and access to the Mass Spectrometry Service and the  
Microanalysis Laboratory at the University of Manchester are  
also acknowledged.

## ■ REFERENCES

- (1) Denniss, I. S.; Jeapes, A. P. In *The Nuclear Fuel Cycle*; Wilson, P. D., Ed.; Oxford University Press: Oxford, U.K., 1986; pp 116–132.
- (2) (a) Nash, K. L.; Choppin, G. R. *Sep. Sci. Technol.* **1997**, *32*, 255–274. (b) Sood, D. D.; Patil, S. K. *J. Radioanal. Nucl. Chem.* **1996**, *203*, 547–573.
- (3) (a) Lanham, W. B.; Runion, T. C. *PUREX process for plutonium and uranium recovery*; USAEC report ORNL-479; Oak Ridge National Laboratory: Oak Ridge, TN, 1949. (b) Warf, J. C. *J. Am. Chem. Soc.* **1949**, *71*, 3257–3258. (c) Batey, W. In *Science and Practice of Liquid–Liquid Extraction*; Thompson, J. D., Ed.; Clarendon Press: Oxford, U.K., 1992; Vol. 2, p 139.
- (4) Paiva, A. P.; Malik, P. *J. Radioanal. Nucl. Chem.* **2004**, *261*, 485–496.

- 1012 (5) Cocalia, V. A.; Jensen, M. P.; Holbrey, J. D.; Spear, S. K.;  
1013 Stepinski, D. C.; Rogers, R. D. *Dalton Trans.* **2005**, 1966–1971.
- 1014 (6) Warin, D. *IOP Conf. Ser.: Mater. Sci. Eng.* **2010**, *9*, 012063.
- 1015 (7) Panak, P. J.; Geist, A. *Chem. Rev.* **2013**, DOI: 10.1021/cr3003399
- 1016 (8) Madic, C.; Hudson, M. J.; Liljenzin, J.-O.; Glatz, J.-P.; Nannicini,  
1017 R.; Facchini, A.; Kolarik, Z.; Odoj, R. *Prog. Nucl. Energy* **2002**, *40*,  
1018 523–526.
- 1019 (9) Madic, C.; Boullis, B.; Baron, P.; Testard, F.; Hudson, M. J.;  
1020 Liljenzin, J.-O.; Christiansen, B.; Ferrando, M.; Facchini, A.; Geist, A.;  
1021 Modolo, G.; Espartero, A. G.; De Mendoza, J. *J. Alloys Compd.* **2007**,  
1022 444–445, 23–27.
- 1023 (10) Hudson, M. J.; Harwood, L. M.; Laventine, D. M.; Lewis, F. W.  
1024 *Inorg. Chem.* **2013**, DOI 10.1021/ic3008848.
- 1025 (11) Grouiller, J.-P.; Pillon, S.; de Saint Jean, C.; Varaine, F.; Leyval,  
1026 L.; Vambenepe, G.; Carlier, B. *J. Nucl. Mater.* **2003**, *320*, 163–169.
- 1027 (12) Geist, A.; Hill, C.; Modolo, G.; Foreman, M. R. St. J.; Weigl, M.;  
1028 Gompper, K.; Hudson, M. J. *Solvent Extr. Ion Exch.* **2006**, *24*, 463–  
1029 483.
- 1030 (13) Nilsson, M.; Nash, K. *Solvent Extr. Ion Exch.* **2007**, *25*, 665–701.
- 1031 (14) Gelis, A. V.; Vandegrift, G. F.; Bakel, A.; Bowers, D. L.; Hebden,  
1032 A. S.; Pereira, C.; Regalbuto, M. *Radiochim. Acta* **2009**, *97*, 231–232.
- 1033 (15) (a) Mincher, B. J.; Schmitt, N. C.; Case, M. E. *Solvent Extr. Ion*  
1034 *Exch.* **2011**, *29*, 247–259. (b) Vandegrift, G. F.; Chamberlain, D. B.;  
1035 Connor, C.; Copple, J. M.; Dow, J. A.; Everson, L.; Hutter, J. C.;  
1036 Leonard, R. A.; Nunez, L.; Regalbuto, M. C.; Sedlet, J.; Srinivasan, B.;  
1037 Weber, S.; Wygmans, D. G. Proceedings of the Symposium on Waste  
1038 Management, Tuscon, AZ, 1993.
- 1039 (16) Brown, J.; Carrott, M. J.; Fox, O. D.; Maher, C. J.; Mason, C.;  
1040 McLachlan, F.; Sarsfield, M. J.; Taylor, R. J.; Woodhead, D. A. *IOP*  
1041 *Conf. Ser.: Mater. Sci. Eng.* **2010**, *9*, 012075.
- 1042 (17) (a) Kolarik, Z.; Mülllich, U.; Gassner, F. *Solvent Extr. Ion Exch.*  
1043 **1999**, *17*, 23–32. (b) Kolarik, Z.; Mülllich, U.; Gassner, F. *Solvent Extr.*  
1044 *Ion Exch.* **1999**, *17*, 1155–1170. (c) Drew, M. G. B.; Guillauneux, D.;  
1045 Hudson, M. J.; Iveson, P. B.; Russell, M. L.; Madic, C. *Inorg. Chem.*  
1046 *Commun.* **2001**, *4*, 12–15.
- 1047 (18) (a) Drew, M. G. B.; Foreman, M. R. S. J.; Hill, C.; Hudson, M.  
1048 J.; Madic, C. *Inorg. Chem. Commun.* **2005**, *8*, 239–241. (b) Foreman,  
1049 M. R. S. J.; Hudson, M. J.; Geist, A.; Madic, C.; Weigl, M. *Solvent Extr.*  
1050 *Ion Exch.* **2005**, *23*, 645–662.
- 1051 (19) (a) Magnusson, D.; Christiansen, B.; Foreman, M. R. S.; Geist,  
1052 A.; Glatz, J.-P.; Malmbeck, R.; Modolo, G.; Serrano-Purroy, D.; Sorel,  
1053 C. *Solvent Extr. Ion Exch.* **2009**, *27*, 97–106. (b) Magnusson, D.;  
1054 Christiansen, B.; Malmbeck, R.; Glatz, J.-P. *Radiochim. Acta* **2009**, *97*,  
1055 497–502.
- 1056 (20) Lewis, F. W.; Harwood, L. M.; Hudson, M. J.; Drew, M. G. B.;  
1057 Desreux, J. F.; Vidick, G.; Bouslimani, N.; Modolo, G.; Wilden, A.;  
1058 Sypula, M.; Vu, T.-H.; Simonin, J.-P. *J. Am. Chem. Soc.* **2011**, *133*,  
1059 13093–13102.
- 1060 (21) Brown, J.; McLachlan, F.; Sarsfield, M.; Taylor, R.; Modolo, G.;  
1061 Wilden, A. *Solvent Extr. Ion Exch.* **2012**, *30*, 127–141.
- 1062 (22) Aneheimmrgt, E.; Ekberg, C.; Fermvik, A.; Foreman, M. R. St.  
1063 J.; Retegan, T.; Skarnemark, G. *Solvent Extr. Ion Exch.* **2010**, *28*, 437–  
1064 458.
- 1065 (23) Foreman, M. R. S.; Hudson, M. J.; Drew, M. G. B.; Hill, C.;  
1066 Madic, C. *Dalton Trans.* **2006**, 1645–1653.
- 1067 (24) Steppert, M.; Cisařová, I.; Fanghänel, T.; Geist, A.; Lindqvist-  
1068 Reis, P.; Panak, P.; Stěpnička, P.; Trumm, S.; Walther, C. *Inorg. Chem.*  
1069 **2012**, *51*, 591–600.
- 1070 (25) Retegan, T.; Berthon, L.; Ekberg, C.; Fermvik, A.; Skarnemark,  
1071 G.; Zorz, N. *Solvent Extr. Ion Exch.* **2009**, *27*, 663–682.
- 1072 (26) Lewis, F. W.; Harwood, L. M.; Hudson, M. J.; Drew, M. G. B.;  
1073 Sypula, M.; Modolo, G.; Whittaker, D.; Sharrad, C. A.; Videva, V.;  
1074 Hubscher-Bruder, V.; Arnaud-Neu, F. *Dalton Trans.* **2012**, *41*, 9209–  
1075 9219.
- 1076 (27) Hubscher-Bruder, V.; Haddaoui, J.; Bouhroum, S.; Arnaud-Neu,  
1077 F. *Inorg. Chem.* **2010**, *49*, 1363–1371.
- 1078 (28) (a) Vacca, A.; Sabatini, A.; Gans, P. *Hyperquad2006*, version  
1079 3.1.48; Protonic Software Corp.: Dallas, TX, 2006. (b) Gans, P.;  
1080 Sabatini, A.; Vacca, A. *Talanta* **1996**, *43*, 1739–1753.
- (29) Natrajan, L. S.; Khoabane, N. M.; Dadds, B. L.; Muryn, C. A.;  
1081 Pritchard, R. G.; Heath, S. L.; Kenwright, A. M.; Kuprov, I.; Faulkner,  
1082 S. *Inorg. Chem.* **2010**, *49*, 7700–7709.
- (30) Pathak, P. N.; Ansari, S. A.; Godbole, S. V.; Dhobale, A. R.;  
1083 Manchanda, V. K. *Spectrochim. Acta A* **2009**, *73*, 348–352.
- (31) (a) Richardson, F. S. *Chem. Rev.* **1982**, *82*, 541–552. 1086  
(b) Natrajan, L. S.; Blake, A. J.; Wilson, C.; Weinstein, J. A.; Arnold,  
1087 P. L. *Dalton Trans.* **2004**, 3748–3755. 1088  
(32) Trumm, S.; Lieser, G.; Foreman, M. R. S. J.; Panak, P. J.; Geist,  
1089 A.; Fanghänel, T. *Dalton Trans.* **2010**, *39*, 923–929. 1090  
(33) Tedeshi, C.; Picaud, C.; Azéma, J.; Donnadiou, B.; Tisnès, P.  
1091 *New J. Chem.* **2000**, *24*, 735–737. 1092  
(34) (a) Beeby, A.; Clarkson, I. M.; Dickins, R. S.; Faulkner, S.;  
1093 Parker, D.; Royle, L.; de Sousa, A. S.; Williams, J. A. G.; Woods, M. J. *1094*  
*Chem. Soc., Perkin Trans. 2* **1999**, 493–503. (b) Zhao, Y.-F.; Zhao, Y.-  
1095 L.; Bai, F.; Wei, X.-Y.; Zhou, Y.-S.; Shan, M.-N.; Li, H.-H.; Ma, R.-J.;  
1096 Fu, X.-T.; Du, Y. J. *Fluoresc.* **2010**, *20*, 763–770. 1097  
(35) (a) Fletcher, D. A.; McMeeking, R. F.; Parkin, D. J. *Chem. Inf.* 1098  
*Comput. Sci.* **1996**, *36*, 746–749. (b) Allen, F. H. *Acta Crystallogr.* 1099  
**2002**, *B58*, 380–388. (c) Bruno, I. J.; Cole, J. C.; Edgington, P. R.;  
1100 Kessler, M.; Macrae, C. F.; McCabe, P.; Pearson, J.; Taylor, R. *Acta*  
1101 *Crystallogr.* **2002**, *B58*, 389–397. (d) Macrae, C. F.; Edgington, P. R.;  
1102 McCabe, P.; Pidcock, E.; Shields, G. P.; Taylor, R.; Towler, M.; van de  
1103 Streek, J. *J. Appl. Crystallogr.* **2006**, *39*, 453–457. 1104  
(36) (a) Cotton, S. A.; Franckevicius, V.; Mahon, M. F.; Ling Ooi, L.;  
1105 Raithby, P. R.; Teat, S. J. *Polyhedron* **2006**, *25*, 1057–1068. 1106  
(b) Kaczmarek, A. M.; Kubicki, M.; Pospieszna-Markiewicz, I.;  
1107 Radecka-Paryzek, W. *Inorg. Chim. Acta* **2011**, *365*, 137–142. 1108  
(c) Merkel, M.; Pascaly, M.; Köster, C.; Krebs, B. Z. *Naturforsch. B* 1109  
**2004**, *59*, 216–220. 1110  
(37) (a) Berthet, J.-C.; Thuéry, P.; Foreman, M. R. S.; Ephritikhine,  
1111 M. *Radiochim. Acta* **2008**, *96*, 189–197. (b) Berthet, J.-C.; Thuéry, P.;  
1112 Dognon, J.-P.; Guillauneux, D.; Ephritikhine, M. *Inorg. Chem.* **2008**, *47*,  
1113 6850–6862. (c) Berthet, J.-C.; Maynadié, J.; Thuéry, P.; Ephritikhine,  
1114 M. *Dalton Trans.* **2010**, *39*, 6801–6807. 1115  
(38) (a) Gregloński, G.; Lisowski, L. *Angew. Chem., Int. Ed.* **2006**, *45*,  
1116 6122–6126. (b) Visinescu, D.; Fabelo, O.; Ruiz-Pérez, C.; Lloret, F.;  
1117 Julve, M. *CrystEngComm* **2010**, *12*, 2454–2465. 1118  
(39) (a) Feng, M.-L.; Mao, J.-G. *Eur. J. Inorg. Chem.* **2007**, *34*, 5447–  
1119 5454. (b) Zhou, X.-H.; Peng, Y.-H.; Du, X.-D.; Wang, C.-F.; Zuo, J.-L.;  
1120 You, X.-Z. *Cryst. Growth Des.* **2009**, *9*, 1028–1035. (c) Zhang, Z.-J.;  
1121 Shi, W.; Huang, Y.-Q.; Zhao, B.; Cheng, P.; Liao, D.-Z.; Yan, S.-P.  
1122 *CrystEngComm* **2009**, *11*, 1811–1814. 1123  
(40) Lam, A. W.-H.; Wong, W.-T.; Wen, G.; Zhang, X.-X.; Gao, S.  
1124 *New J. Chem.* **2001**, *25*, 531–533. 1125  
(41) Sarsfield, M. J.; Taylor, R. J.; Maher, C. J. *Radiochim. Acta* **2007**,  
1126 *95*, 677–682. 1127  
(42) SMART, version 5.625; Bruker AXS Inc.: Madison, WI, 2001. 1128  
(43) SAINT, version 6.36a; Bruker AXS Inc.: Madison, WI, 2002. 1129  
(44) SADABS, version 2.03a; Bruker AXS Inc.: Madison, WI, 2001. 1130  
(45) Altomare, A.; Casciarano, G.; Giacovazzo, C.; Guagliardi, A. J. 1131  
*Appl. Crystallogr.* **1993**, *26*, 343–350. 1132  
(46) Sheldrick, G. M. *SHELXL97, Programs for Crystal Structure*  
1133 *Analysis*, release 97-2; University of Göttingen: Göttingen, Germany,  
1134 **1998**. 1135  
(47) Farrugia, L. J. *J. Appl. Crystallogr.* **1997**, *30*, 565. 1136  
(48) Ravel, B.; Newville, M. J. *Synchrotron Radiat.* **2005**, *12*, 537–  
1137 541. 1138  
(49) Newville, M. J. *Synchrotron Radiat.* **2001**, *8*, 322–324. 1139  
(50) Denecke, M. A.; Rossberg, A.; Panak, P. J.; Weigl, M.;  
1140 Schimmelpennig, B.; Geist, A. *Inorg. Chem.* **2005**, *44*, 8418–8425. 1141